NASA TECHNICAL MEMORANDUM

NASA TM X- 73508

NASA TM X-73508

A 15,000-HOUR CYCLIC ENDURANCE TEST OF AN 8-CENTIMETER-DIAMETER ELECTRON BOMBARDMENT MERCURY ION THRUSTER

by Shigeo Nakanishi
Lewis Research Center
Cleveland, Ohio 44135

TECHNICAL PAPER to be presented at the
Twelfth International Electric Propulsion Conference sponsored by
the American Institute of Aeronautics and Astronautics
Key Biscayne, Florida, November 15-17, 1976

A 15,000-HOUR CYCLIC ENDURANCE TEST OF AN 8-CENTIMETER-DIAMETER ELECTRON BOMBARDMENT MERCURY ION THRUSTER

Shigeo Nakanishi
National Aeronautics and Space Administration
Lewis Research Center
Cleveland, Ohio 44135

E-884

Abstract

A laboratory model 8-cm thruster with improvements to minimize ion chamber erosion and peeling of sputtered metal was subjected to a cyclic endurance test for 15,040 hours and 460 restarts. A charted history of several thruster operating variables and off-normal events are shown in 600-hour segments at three points in the test. The transient behavior of these variables during a typical start-stop cycle is presented. Performance and operating characteristics were nearly constant throughout the test except for a change in the accelerator back-streaming limit.

Findings of the post-test inspection confirmed most of the expected results. Charge-exchange ions caused normal accelerator grid erosion. The workability of the various design features have been substantiated, and attainable improvements in propellant utilization efficiency should significantly reduce accelerator erosion.

Introduction

Long life (5 to 10 yr) geosynchronous spacecraft auxiliary propulsion requirements have spurred interest in demonstrating the durability of low thrust mercury ion thrusters. A 5-cm diameter thruster with ion accelerator optics designed for electrostatic beam vectoring was previously tested for 9715 hours (ref. 1). The test was a demonstration of durability and reliability of an auxiliary propulsion mercury ion thruster. A 10,000-hour life test of a 30-cm diameter thruster designed for primary propulsion applications is reported in reference 2. Life tests on various components have been completed or are currently in progress (refs. 3 and 4). Actual flight testing in space with the SERT II thruster is still possible years after its 1970 launch (ref. 5).

A 1-mlb laboratory model 8-cm beam diameter electron bombardment mercury ion thruster has now successfully completed a cyclic endurance test for 15,040 hours and 460 on-off cycles at the NASA Lewis Research Center. The thruster development program and test extended the knowledge and experience gained from the previous 5-cm thruster test. Several improvements were incorporated into the 8-cm thruster to minimize ion chamber erosion and peeling of sputtered metal observed in the 5-cm thruster. The present test sought to evaluate the effectiveness of these improvements, to determine reliability under a cyclic operating mode, and to identify failure modes not apparent in shorter tests.

Because of the early inception of the test, the specific designs used were preliminary. Test facility and equipment modifications were limited to those which could be made within the time constraint between two successive tests. Shutdown and startup cycling was performed manually, and test observations were made daily.

An interim report of the test was given at about 7400 hours into the test (ref. 6). Presented therein were performance characteristics and some component photographs obtained when the test was interrupted at 1156 hours to replace a delaminated pyrolytic graphite baffle.

Presented in this concluding report are segments of the time history at 5000, 10,000, and the final hours of the test. Transient behavior during a typical start-stop cycle is shown. Performance profiles and operating characteristics from widely separated points in the test are compared. Results of post-test documentation and examination include weight analyses, ion beam profiles, and component photographs. Observed erosion of some of the components are compared with calculated values.

Apparatus and Procedure

A cross-section drawing of the laboratory model 8-cm thruster is shown in figure 1. The cathode-isolator-vaporizer (CIV) and the neutralizer-vaporizer (NV) assemblies were similar to those formerly developed for the 5-cm thruster. The rolled-foil inserts of the cathode and neutralizer were replaced with inserts of the barium-impregnated porous tungsten type. The insert change in the cathode made it necessary to use a coaxial swaged sheath heater for fabrication reasons. The thruster had a 9.4-cm-diameter by 7.77-cm-long anode fabricated of 0.5-mm diameter stainless steel wire screen mesh with 19 wires per cm. The cathode pole piece was a conical vented design with a discharge diameter of 1.59 cm. The vented region was covered with fine tantalum wire mesh. Two cathode baffles were used in the test. The original baffle was 0.63 cm in diameter, 0.28-cm thick, and of anisotropic pyrolytic graphite. A second design was similar to the 5-cm thruster baffle but fabricated of 0.063-cm-thick isotropic graphite instead of tantalum. The graphite baffle was fastened with a flat-head tantalum screw. The thruster backplate was covered with an anisotropic pyrolytic graphite sheet. An auxiliary electrode was mounted through the thruster backplate on a shadow-shielded insulator to allow high voltage pulse ignition of the cathode. The isolator section of the CIV was completely enclosed within the conical support. The larger end of the cone was covered by a pair of overlapping disks to form a reentrant-type contamination shield.

The ion accelerator optics were dished grids with 1.97-mm diameter screen holes on 2.21 mm equilateral triangle centers (72.5-percent open area) and 1.69-mm diameter accelerator holes (53-percent open area). The chickness of both grids was 0.52 mm and the minimum gap between the grids near the thruster axis was 0.51 mm.

Also visible in the figure is the neutralizer mounted with its axis parallel to the thruster axis. The keeper hole was positioned 3.57-cm downstream and 3.54-cm radially outward from the outermost active accelerator grid hole located at a radius of 4 cm. The neutralizer was also equipped with an auxiliary electrode for pulse ignition. The entire

STAR category 20

thruster assembly was covered by a mask and screen enclosure held at neutralizer floating potential. A photograph of the thruster assembly prior to test is shown in figure 2. The rectangular box mounted on a movable rod contained a glass slide to document sputter efflux.

Figure 3 shows the interior of the 1.4-m diameter by 1.8-m high vertical vacuum facility prior to the test. The 1.12-m diameter stainless steel pan for the frozen mercury target was attached to 12 radial copper struts containing brazed copper cooling coils. A helical cooling coil welded to a perforated stainless steel shell formed the cryowall which extended along the vertical wall of the tank.

The thruster was mounted with a distance of 76 cm between the frozen mercury target and the accelerator grid. A set of non-metallic baffles was installed to prevent backsputtering of condensible conductive material from the facility walls. The baffle assembly consisted of three slanted annular baffles spaced 25-cm apart with an 83.8-cm inside diameter opening. The baffles were made from 0.63-cm thick sheets of Fiberfax insulation (50 percent Al_2O_3; 50 percent SiO_2) fitted and supported on a stainless steel frame. The ion beam, therefore, had no line of sight to surfaces other than the frozen mercury and the Fiberfax insulation.

The laboratory-type power supplies and the instrumentation used in the test are described in references 6 and 7. A schematic diagram of the electrical wiring used in the thruster test is shown in figure 4.

The critical supplies, such as discharge voltage and the keeper supplies, had regulation of 1 percent or better and were voltage and current regulated with automatic cross-over. The cathode vaporizer supply could be set manually or switched to accept the discharge voltage as a feedback signal for proportional control about a set point.

All voltages and currents associated with thruster operation were displayed on panel meters. D.C. voltage signals proportional to these measurements were also provided to the central automatic digital data encoder (CADDE) system of the Lewis Research Center. Voltage and current signals floating at cathode potential were transmitted to ground potential by optically coupled d.c. signal isolators. In the present test, an in-line calibration box containing voltage test terminals and standard current shunts permitted periodic on-line calibration of the panel meters and signal isolators. A four-channel strip chart recorder for continuous monitoring of selected variables was also included.

The 8-cm thruster test procedures were essentially similar to those used in the 5-cm test with two exceptions. Duty cycle operation was simulated by week-day runs of $22\frac{1}{2}$ hours on and $1\frac{1}{2}$ hours off. On nonworking days, the thruster was operated continuously. Startup followed the conventional cathode and vaporizer heating procedures, but ignition was obtained by applying 5-kV pulses to the auxiliary electrodes with 40-volts d.c. applied to the keepers. Shutdown was accomplished by a single switch which simultaneously de-energized all power supplies.

The thruster was operated at fixed conditions with minor discharge current adjustments to maintain a beam current of 72 mA. The set point for closed loop control of the discharge voltage was 40 volts. This resulted in an equivalent cathode flow rate of 106 to 117 mA.

The neutralizer vaporizer temperature was manually controlled to maintain a flow rate of 6 to 7.5 mA. This level of flow was selected on basis of preliminary belljar tests which indicated a strong dependence of neutralizer erosion on flow rate.

The cathode was operated without tip heat except during startups. Neutralizer tip heat was adjusted as required to assure stable operation. For most of the test, the neutralizer was operated with 7.2 watts of applied heater power.

The test facility was opened to atmosphere only once at 1156 hours. The thruster was disassembled for photographic documentation and reassembled with a new baffle being the only change.

Results and Discussion

Time History of Test

Three segments of test history, each about 600 hours in length, taken at 5000, 10,000, and 15,000 hours into the test are shown in figure 5. Plotted against time are the four variables most subject to change with time and most indicative of performance degradation. The restart numbers at various points in time are indicated. If there were consistent variations over each on-off cycle, they are not discernible on this time scale. The two types of abnormal event leading to automatic thruster shutdown were neutralizer extinction and high tank pressure. Neutralizer extinction usually occurred without forewarning. Some, however, were preceded by a decline in stability or by grid arcs. Thruster operation without a neutralizer discharge was not possible because of the floating neutralizer. High tank pressure was usually caused by insufficient flow of liquid nitrogen.

Grid arcs were nonexistent, or undetected, until the final 500 hours of the test. The events noted in figure 5 were not single arcs but a series of 3 to 6 current spikes about 1/2 to 1 hour apart recorded on a strip chart. The pattern of these occurrences was a series of current spikes followed by a long period of no arcs. The neutralizer heater power was increased to 14.4 watts at 14,690 hours in an attempt to avoid the frequent neutralizer extinctions. Based on 5-cm thruster experience, series inductive chokes were installed in the outputs of the accelerator and net accelerating potential power supplies at 14,727 hours. These chokes limited the arc current and reduced the number of neutralizer extinctions. Beyond that point to the end of the test, the neutralizer extinguished three times. The third one occurred with the heater power turned down to the normal 7.2 watt level.

The accelerator drain current shown in figure 5(a) was sensitive to both tank pressure and propellant flow rate. Post-test inspection showed that charge exchange ion erosion of the accelerator grid was considerable. Accelerator hole size, however, did not change significantly. The drain current

was therefore concluded to consist almost entirely of charge-exchange ion current and very little direct impingement of beam ions. The mean level of drain current was essentially constant at 0.2 mA until the final hours of the test when an unsteady rise to a maximum level of 0.24 mA was reached.

The variation in cathode keeper voltage with time is shown in figure 5(b). The cathode was operated without tip heater power, but the periodic heating prior to each start may have been helpful in reconditioning the emissive surfaces of the insert. The mean level of cathode keeper voltage was nearly constant at 14 volts, but there were some variations as large as ±2 volts. The increase in keeper voltage was usually associated with a high tank pressure condition and, therefore, a possible poisoning of the cathode emissive surface. The reason for the 2-volt drop in voltage at about 14,900 hours is not known. All thruster variables were at normal levels and no abnormal events preceded the drop in keeper voltage. The sudden increase back to the 14 volt level at 14,930 hours is likewise unexplained, especially because this increase occurred during the same day, intervened only by a normal shutdown and restart.

The neutralizer keeper voltage is shown in figure 5(c). The keeper voltage was essentially constant throughout the life test. This was in contrast to the 5-cm test (ref. 1) in which the voltage gradually increased at a rate of about 1 volt per 1000 hours of operation.

Approximately 7 watts of heater power was required to maintain stable neutralizer operation over a prolonged period. Effects similar to the 5-cm experience were observed with changes in heater power. Increasing the power to twice normal decreased the keeper voltage 3 to 4 volts. Removing all heater power increased the keeper voltage about $4\frac{1}{2}$ volts.

The neutralizer floating potential shown in figure 5(d) exhibited the most variation during the test. There appeared to be about a 5-volt drop in the mean level over each 5000 hours of operation, but random variations of this magnitude also existed throughout the test.

For most of the test, the neutralizer was operated at constant conditions of mercury flow, keeper current, and heater power. As shown in the test history segments (fig. 5) and at other times in the test, heater power ranging from 0 to 14.4 watts was tried for short periods. When low heater power was used, neutralizer stability usually declined within 30 to 48 hours, accompanied by erratic variations in neutralizer floating potential or neutralizer extinction.

Higher heater power was used when the normal 7.2 watts was insufficient to assure steady neutralizer operation. The cause of erratic operation is not clearly known. It has been theorized that an activated emissive surface in the neutralizer insert is necessary, and that some optimum temperature is required to promote the migration or diffusion of barium without excessive loss due to evaporation. Contamination or poisoning could also be more prevalent when the surface temperatures are less than optimum. The experiences of numerous experimenters seem to be consistent with this theory. Some of these tendencies have already been discussed with the cathode keeper voltage behavior.

As shown in the test history, increasing the heater power lowered the keeper voltage and floating potential. Decreasing heater power usually produced the reverse effect. In a cyclic test, the effects of emissive surface degradation are masked by the periodic heating to high temperatures to obtain neutralizer ignition. The insert surface may thus undergo periodic reactivation. This may help to explain the absence of extinction during the zero power period from 10,340 to 10,570 hours.

On the other hand, the period from 14,690 to 14,770 hours encountered numerous neutralizer extinctions even with 14.4 watts of heater power. Some of the extinctions were due to grid arcs. After installation of the chokes, neutralizer heater power was held at 14.4 watts until 14,772 hours when it was reduced by 7.2 watts. Neutralizer operation was relatively stable thence to the end of the test.

Transient Behavior of a Typical Cycle

Transient behavior of a typical cycle from startup to shutdown is shown in figure 6. The data were obtained from the automatic CADDE record at 10,081 hours and 300 cycles into the test. Because the data were scanned and digitized at approximately 40 minute intervals, successive points have been connected by straight line segments.

The five variables plotted were selected as most meaningful in tracking the slow transients. Discharge voltage which was automatically controlled to a set point of 40 volts remained within ±0.2 volt after the first 0.2 hour. For two of the variables, the circled values were obtained from a multi-channel continuous strip chart record which will be discussed presently.

Accelerator drain current shown in figure 6(a) was initially as much as 0.6 mA because mercury which condensed in the ion chamber during preheating, re-evaporated after the thruster was turned on. This caused a period of high neutral density which dropped to normal levels within about 3 minutes of operation. The general trend of the digital data agreed with the strip chart data. The deviations from a mean curve are believed to be caused by digitizing errors resulting from noise in the signal. The gradual rise in the drain current toward the end of the cycle was caused by a rise in tank pressure from an indicated value of 1×10^{-6} to 2×10^{-6} Torr.

The cathode keeper voltage (fig. 6(b)) was not recorded continuously, so only the digital data is plotted. The voltage stayed essentially constant throughout the cycle with a maximum deviation of 0.2 volt from the mean value.

The neutralizer floating potential is shown in figure 6(c). It initially reached about -40 volts because the neutralizer flow rate had not settled down from the prestart value to the normal operating level. The digital data indicated a noisy signal until about 9 hours into the cycle after which it tracked the continuous data very closely. It is not known whether the noise was thruster or facility generated. The potential increased to a peak value of -28.6 volt at about the 7th hour and then gradually decreased to the final value of

about -24 volt. The neutralizer vaporizer temperature was constant within ±1.0° C over the entire period so the variation in floating potential must be attributed to other causes.

The beam and discharge currents are plotted in figure 6(d). As mentioned earlier, propellant flow was controlled to hold a set value of discharge voltage. Discharge current regulation was about ±1 percent. The beam current was adjusted to 72 mA shortly after startup and left to stabilize. At about the 6th hour (end of day) the beam was readjusted to 72 mA and left overnight. Over the ensuing 15 hours, the beam current remained essentially constant at 72 mA, but discharge current drifted down from 0.73 to 0.72 A. This current drift was within the regulation limit of the power supply. Thruster performance apparently stabilized or improved sufficiently so that output beam current was not affected by the downward drift in discharge current. It is also possible that the slight increase in tank pressure indicated by the rising accel drain current contributed to a change in both output beam current and neutralizer coupling.

A continuous strip chart record of the same cycle is shown in figure 7. The four variables charted, their scale factors, and relative pen positions are indicated. The entire sequence starting with neutralizer vaporizer preheat 20 minutes prior to beam burn-on is shown by the rapid rise in vaporizer temperature. The cathode and cathode vaporizer were heated during the same period. The preheating period was followed by neutralizer and cathode ignition in quick succession.

Beam turn-on caused a steep rise in accel drain current. Neutralizer vaporizer power was reduced to the normal run level as indicated by the rapid drop in vaporizer temperature. As mentioned previously, the re-evaporation of condensed mercury in the ion chamber caused accelerator drain current, presumably charge exchange current, to rise to about 0.65 mA and then drop rapidly within about 3 minutes to 0.2 mA, the normal operating level.

During the initial half-hour after starting, the accel drain current signal showed fluctuations ranging from -19 to +14 percent of the mean value. Simultaneously, but apparently 180° out of phase, the discharge voltage showed variations of about ±10 percent of the mean value.

As operation progressed into the first and second hour the disturbances in the discharge voltage and drain current became less frequent. By the 7th hour the disturbance rate decreased to approximately once in 2 hours and to once in 3 hours by the 19th hour. The cause of these disturbances is not known, but they are believed to originate in the ionization chamber rather than in the accelerator optics.

The neutralizer floating potential generally followed the trend discussed previously under the digitized record. The disturbances evident in the discharge voltage and drain current also affected the floating potential but to a much lesser degree (approx. 4 percent). The absence of spurious variations in the digitized signal after the 9th hour is also in agreement with the sparseness of the disturbances beyond that hour in the cycle. The amplitudes by which the disturbances departed from the mean values of the floating potential and drain current were of the same order of magnitude as the spurious variations in their digitized signals.

Performance Profile

Table I shows the thruster performance profiles evaluated at 5500, 10,000, and 15,000 hours. The net accelerating and accelerator potentials were not always the same because of slight maladjustments of the power supplies. Cathode and neutralizer flow rates also deviated because of the difficulties in pre-setting a precise flow value. The beam current was manually adjusted to 72 mA each time using a digital meter, so the variations in beam power resulted from variations in the net accelerating potential. Other component powers were either equal or compensating so that the power efficiency was uniform within 1 percent for all three times.

The cathode flow rate was preset somewhat lower at the 15,000-hour point than either of the previous two times. Propellant utilization efficiency and overall efficiency were consequently highest at 15,000 hours. Also because of the utilization and net accelerating potential, the specific impulse at 15,000 hours was the highest of the three times. These higher values do not reflect an improvement in performance with time. They indicate the typical sensitivity of these performance parameters to the governing thruster variables, and also show that the thruster operating characteristics did not degrade appreciably with time.

Thruster Characteristics

Cathode keeper current. - The effects of varying cathode keeper current while adjusting discharge current to maintain a 72-mA beam current are shown in figure 8. The discharge current (fig. 8(a)) and keeper voltage (fig. 8(c)) characteristics were essentially unchanged between 5500 and 15,000 hours, except for a small shift in levels. The discharge voltage (fig. 8(b)) was characteristically higher at 15,000 hours, because of the lower propellant flow rate. It should be noted that during these mapping runs, the propellant flow control loop was opened so that changes in discharge voltage did not change input power to the vaporizer. A delayed thermal feedback from the cathode to the vaporizer, however, could eventually cause a drift in vaporizer temperature and hence, flow.

Discharge current. - The effects of varying discharge current while holding a constant cathode keeper current are shown in figure 9. After about 6000 hours into the test, it was found that a cathode keeper current of 0.20 A was preferable to the 0.24 A used previously. The lower value was, therefore, used for the balance of the test.

During steady-state operation, the discharge current was the governing variable used to adjust beam current to the 72 mA level. The discharge voltage (fig. 9(a)) was about 4 volts higher at 15,000 hours because of the lower propellant flow rate (106 mA vs. 115 mA at 5500 hr). Except for the isolated points at 0.2 A discharge current, the functional relationship between current and voltage, including the inflection, in the curve, was similar at both times.

The beam current-discharge current relationship (fig. 9(b)) was also similar at 5500 and 15,000 hours. The 72-mA beam current was obtained at a lower value of discharge current (0.61 vs.

0.65A) because of the higher discharge voltage.

Net accelerating potential. - The variations in accelerator drain current and the discharge current with varying net accelerating potential are shown in figure 10. The accelerator voltage was increased to -600 volt for the 15,000-hour mapping to assure that electron backstreaming into the thruster would not occur past the accelerator grid visibly eroded by charge-exchange ions.

The effects of varying net accelerating potential upon accelerator drain current are shown in figure 10(a). Only a single curve is drawn through the 5500- and 15,000-hour points because whatever differences may have existed appeared to be within the data scatter. The drain current increased approximately 10 percent for every 1000 volts increase in net accelerating potential. Because beam current and propellant flow were held constant during the potential change, the change in drain current is presumed to be the result of focusing or impingement effects.

The discharge current plotted in figure 10(b) shows a decreasing trend with increasing net accelerating potential. This effect is attributed to the improved extraction of ions out of the ion chamber via higher effective extraction sheath area.

Accelerator voltage. - The effects of varying accelerator voltage are shown in figure 11. The net accelerating potential was held at 1250 volts. The accelerator drain current at constant beam current shown in figure 11(a) exhibited a slightly decreasing trend with increasing voltage.

The variations in discharge current with accelerator voltage are shown in figure 11(b). In a manner similar to the net accelerating potential, the discharge current required to produce a constant 72 mA beam increased with decreasing accelerator voltage down to 485 volts. At voltages less than 485 volts, the required discharge current decreased. This abnormal decrease is attributed to electron backstreaming past regions of the accelerator where erosion reduced the negative potential barrier. Backstreaming did not occur at 5500 hours as indicated by the continued increase in discharge current required to obtain the 72 mA beam current at lower accelerator voltages.

Backstreaming limit was also defined by the alternate method of varying the accelerator voltage while holding discharge current constant. The results are shown in figure 11(c). As the accelerator voltage was reduced below 550 volts, the beam current dropped slightly because of reduced ion extraction. Further reduction in voltage caused the beam current indication to increase because of electron backstreaming. The limit appeared to be between 450 and 500 volts which agreed with the limit defined in figure 11(b).

Neutralizer keeper current. - Because most of the test was run at a heater power of 7.2 watts, the effects of varying neutralizer keeper current are shown in figure 12 for that power level only. Other values of heater power shifted the curves upward or downward depending on whether the heater power was decreased or increased.

The keeper voltage in figure 12(a) characteristically decreases with increasing keeper current. This trend was typical throughout the test, and the slope of the curve was greater at zero heater power and low keeper currents. A 1-volt decrease in the level of keeper voltage was apparent between 5500 and 15,000 hours, but the data at 10,000 hours was essentially the same as at 15,000 hours.

The variation in neutralizer floating potential with keeper current is shown in figure 12(b). Again, the steep rise with decreasing keeper current was typical throughout the test. Noticeable differences existed in the levels, however. The shift with time was to lower values and hence in a favorable direction. All operating parameters including the neutralizer flow rates were nearly equal at all three times. Also, the 10,000-hour data was approximately midway between 5500 and 15,000 hours. A post-test inspection of the neutralizer tip showed a natural chamfering of the surface in the vicinity of the aperture. Allowances must be made for small flow variations and data scatter, but it is conjectured that rather than a flat-face, the chamfered tip may be more desirable for good neutralizer operation. Hollow cathodes with chamfered tips have been the standard design for the 5- and 8-cm thrusters and this feature will be used in the Engineering Model Thruster.

Ion Beam Profiles

After shutdown of the test, normal erosion of the accelerator grid by charge exchange ions was readily apparent. Some erosion of the grid holes was also evident. To assess the possibility of ion beam defocusing due to accelerator erosion, beam profile measurements were made after the test.

The test facility used for beam profile measurements is described in reference 6. Because this facility was not completed at the time the 15,000-hour life test began, no beam measurement was made prior to the test. For additional post-test documentation, the accelerator grid system from the life test was mounted on a thruster similar to the life test thruster. The grid set was mounted as an integral unit without any change in gap setting. The thruster was then operated at conditions used throughout the life test while obtaining beam profiles. The beam probe was a single molybdenum planar probe 0.63 cm in diameter which swept in a 11-cm radius arc through the thruster centerline.

Comparison with small-hole optics. - Figure 13 is a comparison of the ion beam profiles obtained with two grid sets. One grid set was from the 15,000-hour test. The second grid set used for comparison was a small-hole-accelerator-grid (SHAG) of the type used on the engineering model 8-cm thruster (ref. 8). The beam profile was taken at an axial distance 12.7-cm downstream of the accelerator.

Although the data shown were taken in two different tests, the beam profiles produced by the two grids were not greatly different. The amount of beam divergence indicated by the side wings of the profiles dropped to comparable values at similar radial distances. Also included along the abscissa is a scale indicating the angle corresponding to each radial location measured from the thruster centerline. For near-field profiles, the ion beam source cannot be approximated by a point source. The angle, therefore, is only a geometrical parameter and not truly representative of beam divergence angle which is much smaller.

Detailed studies of ion optics (ref. 9) indicate that beam divergence angle is relatively independent of accelerator hole size when the ratio of accelerator to screen grid hole diameter is greater than about 0.5. The SHAG optics used for comparison had accelerator holes ranging from 0.61 to 0.76 mm in diameter and screen holes of 1.83-mm diameter. Although the ratio of accelerator to screen hole diameters was slightly less than 0.5 in the SHAG optics, the resulting beam profile was similar to that of the 15,000-hour test grid. It may be concluded, therefore, that the beam profile of the 15,000-hour thruster was essentially constant throughout the test. Qualitatively, this conclusion is supported by the similarity of the sputter erosion pattern of the frozen mercury target after each melt and refreeze at different points throughout the test. It can also be concluded, that unless the initial accelerator grid hole diameter is less than one-half the screen hole diameter, subsequent accelerator hole erosion should not greatly affect the ion beam divergence.

Life-test grid. - Figure 14 shows ion beam profiles at three axial locations downstream of the accelerator. The 1.59-cm distance was the closest possible approach to the accelerator before mechanical interference with the ground screen mask.

The ion current measured at an axial distance of 1.59 cm decreased to zero slightly beyond the 8-cm diameter of the active grid region. It should be noted that with the 0.63-cm diameter probe located at the 4-cm radial position, the trailing edge of the probe was still slightly within the beam edge. Also because of some divergence in the beam, at axially downstream distances, the beam diameter was broader.

An unexpected feature of the near profile was the asymmetry near the centerline. The planar probe swept across the grid in an arc but for small angles on either side of center, the traverse was essentially on a diameter. The current density was 2.53 mA/cm^2 at the centerline, and increased to 2.85 mA/cm^2 at a radial distance of about 0.5 cm off center on one side. At the same radial distance on the other side of center, the current density was 2.67 mA/cm^2. The cause of this asymmetry is not known. The cathode baffle is too far upstream in the ion chamber for this scale of nonuniformity to persist in the discharge plasma. It is conjectured that local variations in the grid spacing or some factor increasing the perveance could result in a localized high ion extraction. These geometrical factors pertain to hot running conditions and, therefore, do not necessarily correspond to cold bench measurements. The plausibility of optics-related causes is also supported by the fact that the beam profile changed with axial distance.

Also shown in figure 14 are beam profiles obtained at 5.08 and 12.7 cm downstream of the accelerator. An apparent beam edge indicated by zero current density had diverged an average of 1.95-cm radially in an axial distance of 3.49 cm or 5.3 cm in 11.11 cm to result in a divergence angle of 25° to 29°. This is within the range of angles predicted by reference 9.

At an axial downstream distance of 12.7 cm, the ion beam profile had become practically axisymmetric. Because of beam divergence, the peak density at the centerline decreased to about 1.9 mA/cm^2. A numerical integration of the averaged beam density assuming axial symmetry agreed with the output beam current of 72 mA within 2 percent. The thrust factor, or integral of the cosine components was found to be about 0.95 although this is not too meaningful at close distances.

Post-Test Inspection

Initial cursory inspection after the test revealed the thruster assembly to be in remarkably good condition. The ground screen surfaces and neutralizer assembly were clean and free of the back-sputtered material commonly found in tests without a mercury target. Detailed inspection and documentation proceeded with disassembly. Instead of presenting all documental results, the discussion will be limited to those components which showed erosion or degradation. The intent is to provide an evaluation of the concepts tested as well as to formulate inputs for future design.

Weight analysis. - A comparison of component weights after 1156 and 15,040 into the test is presented in table II. The weight change in grams is tabulated as + or - for gain or loss. Because sputtering is a suaface phenomenon, the relative weight losses are not meaningful unless compared on some scale normalized to the active exposed surface area. Complex geometry precludes a simple comparison. Some general observations and conclusions can be made, however.

The accelerator grid and mount ring lost weight as expected because of the erosion from charge-exchange ions. The gain in screen grid and mount ring weight indicates that the peripheral sputter deposition probably exceeded the loss of material due to central erosion. The anode gained weight because it received sputtered material without undergoing significant ion sputtering itself due to its positive potential relative to the ion chamber plasma. All components normally at cathode potential lost weight except the thruster body and screen grid and mount ring. The thruster body was also at cathode potential, but it was receiving sputtered material without undergoing much ion bombardment because of locally low ion density and shielding effects of the anode.

The neutralizer ignitor was at neutralizer floating potential which was negative with respect to ground. It probably received charge exchange ions or plasma ions from outside the accel-decel potential well and from the neutralizer discharge itself.

Accelerator grid. - A photograph of the downstream face of the accelerator grid is shown in figure 15. Close-up photographs will more clearly show the character of charge exchange ion erosion. The region of greatest erosion was near the thruster centerline where profile measurements show the highest beam density. A slight amount of circular grooving occurred on the accelerator mounting ring along the inner edge of the ground screen mask (fig. 2). The grooving is believed to be caused by low energy ions produced in regions downstream of the accelerator grid and focused by the ground screen. Neutralizer ions are excluded inasmuch as the erosion near the neutralizer location was not greatly different from other peripheral regions.

A series of photographs is shown in figure 16

which are close-ups of the accelerator holes along a nearly diametrical line. The equilateral triangular array affords the possibility of photographing along any of three straight-line rows of holes. The one selected included the two web regions which suffered the most erosion. The holes along this line are shown in figure 16(a) and marked with numerals running from either side of center.

The photographs are arranged in sequence from left to right starting with number 19 at the edge and decreasing to 1 near the center, then moving to the right from 1 to 18. The central hole was unmarked but will be designated 0. For scaling purposes, a metric rule with millimeter markings is included at the same magnification. As the photographs show, accelerator hole erosion was not apparent until about hole number 13 or 12 (fig. 16(d)). This corresponded to a radial distance of about 2.7 cm. The accelerator hole diameters at this radius, within measurement accuracy, were equal to the diameter of an inactive hole shielded by the screen grid mask (see fig. 15). Visible erosion in holes number 12 and 11 appeared as a downstream chamfer, possibly by highly divergent ions. The erosion caused by charge-exchange ions characteristically focused into the potential well of the web region was not noticeable until hole number 10 or 11. This corresponded to a radial distance of 2.2 cm where a near grid ion beam current density of about 1.8 mA/cm^2 existed. From that radial distance inward the charge exchange erosion increased. At hole number 4 (fig. 16(f)) or 0.88 cm radius, a neighboring web region was eroded through. More holes were eroded as the center was approached.

As shown in figure 16(g) the geometrical center of the accelerator grid was a web between two holes indicated by the pointer. The worst erosion occurred at about holes number 1 and 4 to the right of center (figs. 16(g) and (h)) where enlarged charge exchange pits had eroded completely through. This corresponded to a radial distance of 0.4 to 0.8 cm. Examination of the near-grid beam profile of figure 14 shows that the peak in the ion beam current density occurred, not at the center but between 0.4 and 0.8 cm off center. The left of center in figure 14 does not coincide with the left of center along the photographic traverse, but the radial distances apply. Unexplainable anomolies exist in the erosion pattern. The web region directly above right hole number 1 in figure 16(g) was eroded most. The second most eroded web was between hole 3 and 4 in figure 16(h). These web regions are about 0.6 cm apart, a distance which spans at least two web regions. If indeed the maximum erosion was caused by a localized peak in beam current density, the smaller erosion of the intervening webs between two badly eroded web regions is difficult to reconcile. A calculation of erosion rate based on a model similar to one suggested in reference 10 is presented in appendix A. The results indicate that for the best known values of variables assumed, the amount of erosion observed in 15,000 hours of operation is realistic. Sharply localized erosion, however, might be attributable to localized non-uniformities in ion and neutral densities and electrostatic fields.

Proceeding to the right of center in figure 16 the charge-exchange ion erosion became negligible by hole number 12 (fig. 16(j)). The downstream edges of the holes at this radial location (2.7 cm) appeared chamfered as was observed in the left half of the traverse. The diameter of the holes lying between the grid center and 2.7 cm radius ranged from 1.6 to 1.7 mm. The diameter of the inactive holes on the extreme right (fig. 16(l)) were 1.6 cm.

It is clear from examination that the erosion of the accelerator was due almost entirely to charge exchange ions. Direct impingement erosion appeared to be most noticeable as a chamfering of the downstream edge of the accelerator holes located at about one-half radius from the center. Calculations indicate that if propellant utilization efficiency of the ion chamber had been 89 percent obtainable in the Engineering Model Thruster with SHAG optics (ref. 11) instead of the 65 percent in the test, a comparable degree of erosion, even with the localized high beam current density, would require 66,000 hours of operation to obtain the same degree of wear.

Screen grid. - The upstream, or ion chamber side of the screen grid is shown in figure 17. There was no perceptible erosion and the beam hole diameter at the centerline was equal to the initial value of 1.97 mm. The grid thicknesses at the centerline and at the outer edge was 0.50 and 0.52 mm, respectively.

Considerable amounts of powder and small flakes of sputtered metal can be seen collected in the grid periphery, corresponding to the anode diameter, and the annulus between the anode and the thruster shell. This accumulation is believed to have originated from ion chamber sputtered metal which collected on the screen anode and thruster shell. The anode and thruster shell were not roughened by grit-blasting and adherence of sputtered metal was not firm. The screen anode, however, was effective in controlling the size of spalled sputtered metal. The Engineering Model Thruster will use a fine-mesh screen anode and grit-blasting on all ion chamber surfaces.

Screen anode. - A photograph of the upstream or cathode end of the screen anode is shown in figure 18. The anode showed no evidence of flaking metal. The inner surface of the anode was covered with a black glossy deposit, circumferentially uniform but more heavy on the upstream end. This deposit is believed to be mostly sputtered graphite, from both the baffle and the backplate.

Thruster backplate assembly. - The thruster backplate and cathode pole-baffle assembly is shown in figure 19. The graphite covering on the backplate, although different in appearance when new, varied in thickness only 0.10 mm from the edge to the thinnest region indicating only slight possible erosion. The tantalum mesh covering the mild steel cathode pole piece was intact. The pole piece was visibly eroded only where imperfect fabrication failed to cover the mild steel. An enlarged drawing of the graphite baffle and tantalum tack is shown in figure 20. The broken line denotes the outline when new. The tantalum tack suffered no measurable erosion. The ion chamber side of the graphite baffle eroded about 0.381 mm, or more than half of the original thickness. The diameter of the baffle was eroded to 5.93 mm, or uniformly about 0.21 mm on the radius. The sputter erosion occurred at a nearly uniform rate on the side and edges.

A sputter erosion calculation performed for the

baffle is presented in appendix B. It should be noted that a number of assumptions were necessary. Because a precise value for sputtering yield of singly charged low energy mercury ions on graphite was not available, it was assumed to be of the same order of magnitude as for iron and molybdenum (refs. 12 and 13). For doubly charged mercury ions accelerated across 40 volts, the sputtering yield was assumed to be about 1.5×10^{-2} atoms/ion (ref. 12).

The calculated thickness of erosion was about 0.18 to 0.32 mm compared to the 0.38 mm observed. The same assumptions applied to tantalum, whose sputtering yield is also low, gave erosion values of 0.35 to 0.63 mm which do not agree with the test results. In experimental erosion studies on a 30-cm thruster (ref. 14), the measured and calculated erosion rates for graphite, iron, molybdenum, and copper baffles were in good agreement. Tantalum was an exception showing a measured erosion rate much less than predicted by calculations. The explanation for the discrepancy with tantalum in the 15,000-hour test is not known. The trend found is at least consistent with that of reference 14 and credible in view of the uncertainties and assumptions involved. The Engineering Model Thruster is designed with either solid or flame-sprayed tantalum on ion chamber surfaces subject to sputter erosion.

Cathode. - A photograph of the cathode assembly is shown in figure 21. A few large flakes were found attached to the tantalum keeper cap. Because this surface will be grit-blasted in the Engineering Model Thruster, flaking from this surface should not occur in the future.

The cathode tip utilized a 0.25-mm diameter aperture and a 45° half angle chamfer. Photomicrographs of the cathode tip at the magnifications indicated are shown in figure 22. For comparison, photomicrographs of the cathode after 1156 hours of operation are shown in figure 23. Some fine-scale erosion is evident at the face of the cathode tip and along the chamfer. At the juncture of the cathode aperture and the chamfered surface, somewhat deeper grained erosion occurred. This erosion is clearly visible at the highest magnification. The cathode aperture at its smallest diameter measured about 0.28 mm, not greatly different from the initial 0.25 mm.

Isolator. - In the 5-cm as well as the 8-cm thruster design, the isolator separating the vaporizer from the positive high voltage of the thruster has been integrated into a single cathode-isolator-vaporizer (CIV) assembly. In numerous component tests, both 8- and 30-cm thruster CIV's have demonstrated reliability against a high voltage breakdown through the internal structure of the isolator. A noncatastrophic failure mode, however, has been the development of a leakage current along the external surface of the isolator ceramic body. Investigations (refs. 4) have pointed to numerous contaminant sources such as metal migration, brazing, and spot welding operations during fabrication as well as poor test facility vacuum. The reentrant type shield shown in figure 1 used no brazing or spot-welding and was designed to minimize the possibility of contamination.

Throughout the 15,000-hour test, the isolator was impressed with the nominal 1250-volt net accelerating potential. During each 1000-hour performance mapping operation, the potential was raised to 1300 volts for brief periods. Up to about 11,000 hours into the test the isolator leakage current was always less than 1 microampere. At 10,946 hours the test facility automatically shut down when a heater element failed in the oil diffusion pump. A high pressure excursion followed. After restart, the isolator leakage current appeared normal until 11,080 hours when 1 microampere current was noted. The leakage gradually increased to a maximum of 49.3 microamperes at 12,656 hours after which it decreased slightly, and varied from 32.5 to 46.5 microamperes at the end of the test.

Post-test inspection withoug removal of the thruster revealed a considerable amount of sputtered contamination on one of three ceramic insulators used to support the thruster body. Lack of space and mechanical interference had prevented the use of adequate shielding on this one support. With the thruster in place and without displacing the CIV, the supports were replaced.

The thruster assembly with new supports was re-installed in the test facility for a verification test. Throughout 24 continuous hours of that test the leakage current was no greater than 0.2 microampere, thus indicating that the high leakage current was across the mounting insulator.

Neutralizer. - The neutralizer assembly used in the thruster, photographed after the test, is shown in figure 24. All component parts were in excellent condition. No erosion was evident because the neutralizer keeper cap was well outside the region of any significant ion beam impingement.

Photomicrographs ofthe neutralizer tip at magnifications of ×7.5, ×22.5, and ×52.5 are shown in figure 25. For comparison, corresponding photographs taken at 1156 hours are shown in figure 26. Slight surface erosion of the flat-face tip (about 0.102 to 0.127 mm), and a chamfering effect in the vicinity of the aperture is visible. The aperture diameter after 15,040 hours was about 0.36 mm compared with 0.34 mm at 1156 hours. This contrasted sharply with the neutralizer of the 5-cm diameter ion thruster test in which the aperture eroded to about twice the original diameter in 10,000 hours.

An erosion rate based on measured erosion over 13,884 hours yields 8×10^{-10} cm^3/hr which is in good agreement with 1×10^{-9} cm^3/hr obtained in reference 15.

Concluding Remarks

A laboratory model 8-cm mercury bombardment ion thruster was successfully endurance tested in a cyclic mode for 15,040 hours and 460 restarts. No detrimental erosion or thruster performance change occurred during this test. The test was concluded without a failure, and all thruster components were functioning normally at the end. Performance profiles and operating characteristics evaluated throughout the test were consistent with the test history indications of little or no change except the backstreaming limit which increased because of accelerator erosion and the neutralizer floating potential which decreased slightly with time.

Post-test weights of most thruster components agreed with expected trends of gain and loss. The accelerator grid suffered a normal amount of erosion

from charge exchange ions. An improvement in discharge chamber propellant utilization efficiency from the present 65 percent to better than 89 percent in the Engineering Model Thruster is expected to more than quadruple accelerator life. Erosion of accelerator hole size from direct ion impingement was minimal and beam profiles after 15,000 hours of operation were similar to the beam profile produced by a typical small-hole-accelerator-grid.

This test incorporated and substantiated thruster design changes that evolved from a prior 9715-hour test of a 5-cm thruster. An anode fabricated of wire mesh screen was successful in controlling the spalling and size of sputtered metal flakes. Tantalum was found to be preferable to graphite as a sputter-resistant metal. Neutralizer tip erosion was minimal, confirming earlier test results of reduced erosion at mercury flow rates of 5 mA or more. In view of present test results and other information available for translation into design, the Engineering Model Thruster life expectancy is predicted to be in excess of 20,000 hours.

Appendix A - Charge-Exchange Ion Erosion

For N_i incident ions traveling through a medium of average number density n_0, and charge-exchange cross-section σ, the number of ions that have been charge-exchanged in a distance, x, is given by

$$N(x) = N_i\left(1 - e^{-n_0\sigma x}\right) \qquad (1)$$

For

$$n_0\sigma x \ll 1,\ e^{-n_0\sigma x} \approx 1 - n_0\sigma x$$

Therefore

$$\frac{N(x)}{N_i} = n_0\sigma x \qquad (2)$$

Since the number of singly-charged ions passing or produced per unit time is proportional to their respective currents,

$$\frac{N(x)}{N_i} = n_0\sigma x = \frac{J_A}{J_B} \qquad (3)$$

where

J_A = accelerator drain current due to charge-exchange ions

J_B = beam current

If the accelerator drain current is assumed to be due only to charge-exchange ions, an average value of charge-exchange distance, l, can be defined as

$$l = \frac{J_A/J_B}{n_0\sigma} \qquad (4)$$

For typical values found in the thruster test,

$$J_A/J_B = 0.00278$$

$$n_0 = \frac{(J_0 - J_B)}{A_0 ev} = 4.46\times10^{11}\ \frac{1}{cm^3}$$

where

J_0 = equivalent neutral flow into thruster, 0.110 A

J_B = beam current, 0.072 A

A_0 = accelerator grid open area = $0.53 \times \pi \times (4)^2$ = 26.6 cm^2

e = electronic charge, 1.6×10^{-19} coulomb

v = thermal velocity of neutral Hg, 2×10^4 cm/sec

σ = 6×10^{-15} cm^2

therefore, l = 1.04 cm, the average charge-exchange distance.

In a local grid area consisting of three holes on equilateral triangular spacing, the charge-exchange region is assumed to be the three shaded circular sectors extending for distance, l, and containing un-ionized neutrals and incident ions. All charge-exchange ions produced within the charge-exchange region are assumed to fall upon the accelerator electrode included in the triangle (sketch A).

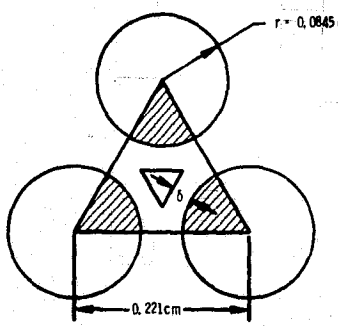

Sketch A

Applying the charge-exchange equation to this region,

$$I_{C.E.} = I_B\sigma n_0 l = j_B A\sigma n_0 l \qquad (5)$$

where

$I_{C.E.}$ = charge-exchange current falling on the grid region

I_B = ion beam current attributable to the region

j_B = local ion beam current density, A/cm^2

$A = 3\left(\frac{\pi r^2}{6}\right) = 0.0112$ cm^2

Ion beam profile measurements have shown current density as high as 0.00285 A/cm^2 measured with a probe 1.59 cm downstream of a grid having 53 percent open area. By continuity, the current density at a beam hole is 0.0054 A/cm^2. An ion beam current of 0.072 A averaged over a grid area 4 cm in radius and 53 percent open fraction yields

$$j_B = \frac{0.072}{\pi \times 4^2 \times 0.53} = 0.0027\ A/cm^2$$

For a typical beam profile, the maximum current density could be twice the average value which agrees with the measured peak density at a beam hole.

Using the maximum current and the beam hole area attributable to the charge-exchange region,

$$I_B = j_B A$$

$$= 0.0054 \times 0.0112 = 6.05\times10^{-5} \text{ A}$$

Using the previous assumptions of uniform unionized efflux and average charge-exchange distance,

$$I_{C.E.} = 6.05\times10^{-5} \times 6\times10^{-15} \times 4.46\times10^{11} \times 1.04$$

$$= 1.68\times10^{-7} \text{ A}$$

Sputtered material mass, M_S

$$M_S = Y_S \times \frac{I_{C.E.}}{e} \times w \times T \qquad (6)$$

where

M_S = sputtered mass, g

Y_S = sputter yield of Hg^+ on Mo = 0.5 atom/ion for 500 V ions

$I_{C.E.}$ = charge-exchange current, A

w = mass of molybdenum atom = 16.1×10^{-23} g/atom

T = time of test = 5.4×10^7 sec = 15,000 hr

$$M_S = \frac{0.5 \times 1.68\times10^{-7} \times 1.61\times10^{-22} \times 5.4\times10^7}{1.6\times10^{-19}}$$

$$= 4.56\times10^{-3} \text{ g}$$

Observation shows that erosion occurs in a triangular pattern between the holes (see fig. 16(g)). The amount of locally eroded material can be related to the thickness, δ, remaining before the eroded region touches a beam hole (see sketch A).

For a grid thickness of 0.052 cm, the results are:

δ		Eroded area, cm^2	Eroded mass, g
in.	cm		
0.017	0.043	0	0
.010	.025	.0017	.0009
.005	.0125	.00486	.0026
.003	.0076	.00655	.0035
.001	.0025	.00856	.0045

The exact pattern of erosion is somewhat different from the idealized pattern but the locally eroded mass for a web region that was almost gone agrees well with the calculated sputtered material mass, M_S. Certain simplifications and convenient relations are possible using the above model and assumptions:

The charge-exchange current falling on a unit equilateral triangular region is

$$I_{C.E.} = I_B \sigma n_0 l$$

where

I_B = ion beam current through the three circular sectors of radius, r

$$= j_B \times 3 \times \frac{\pi r^2}{6}$$

$$= \frac{1}{2} \pi r^2 j_B$$

j_B = the ion beam current density measured by a probe of finite area at a station downstream of the accelerator and adjusted by continuity considerations to the beam hole region

or

j_B = a peak current density inferred by the flatness parameter, P_f, and adjusted by continuity considerations (when beam current density measurements are not available)

Using a measured ion beam current density, j_P

$$j_B = \frac{j_P}{f}$$

where f = open area fraction of the accel grid. Then,

$$I_B = \frac{\pi r^2 j_P}{2f} \qquad (7)$$

From the geometry of a unit equilateral triangular charge-exchange region, having holes of radius, r at the vertices and side, s, the open area fraction, f is

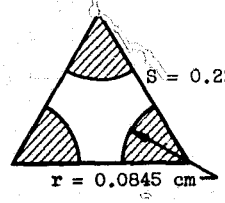

$$f = \frac{3 \times \frac{\pi r^2}{6}}{\frac{1}{2} S^2 \sin 60^\circ}$$

$$f = \frac{\pi r^2}{S^2 \sin 60^\circ} \qquad (8)$$

Substituting in equation (7) for I_B

$$I_B = \frac{j_P S^2 \sin 60^\circ}{2} \qquad (9)$$

For the present values when

$$j_P = 2.85\times10^{-3} \text{ A/cm}^2$$

$$S = 0.221 \text{ cm}$$

Then,

$$I_B = 6.027\times10^{-5} \text{ A}$$

If the peak current density is inferred from the flatness parameter, P_f, which is defined for an active grid area of radius, R as,

$$P_f = \frac{J_{B,avg}}{J_{B,peak}} = \frac{J_B/\pi R^2}{J_{B,peak}} \qquad (10)$$

The current density, j_p, to be used in equation (7) becomes

$$j_p = \frac{J_B/\pi R^2}{P_f}$$

Substituting in equation (7) for I_B,

$$I_B = \frac{J_B}{2fP_f}\left(\frac{r}{R}\right)^2 \qquad (11)$$

Using the equation for charge-exchange current,

$$I_{C.E.} = I_B \sigma n_0 l$$

Remembering that

$$l = \frac{J_A/J_B}{n_0\sigma}$$

$$I_{C.E.} = \frac{j_p S^2 \sin 60^\circ}{2}\frac{J_A}{J_B} \qquad (12)$$

when using a measured ion beam current density, j_p, or

$$I_{C.E.} = \frac{J_A}{2fP_f}\left(\frac{r}{R}\right)^2 \qquad (13)$$

when using the flatness parameter, P_f, and open area fraction f. Note that equation (13) is applicable only at the peak where the flatness parameter is defined. For self-consistent known parameter values in the present case,

$J_A = 2\times10^{-4}$ A

$J_B = 0.072$ A

$S = 0.221$ cm

$f = 0.53$

$P_f = 0.5$

$r = 0.0845$ cm

$R = 4$ cm

$j_p = 2.85\times10^{-3}$ A/cm^2 measured by a probe

Using measured current density from a probe,

$$I_{C.E.} = \frac{j_p S^2 \sin 60^\circ}{2}\times\frac{J_A}{J_B}$$

$$= \frac{2.85\times10^{-3}\times 0.221^2\times \sin 60^\circ}{2}\times\frac{2\times10^{-4}}{0.072} = 1.68\times10^{-7}$$

Using the flatness parameter and drain current,

$$I_{C.E.} = \frac{J_A}{2fP_f}\left(\frac{r}{R}\right)^2$$

$$= \frac{2\times10^{-4}}{2\times 0.53\times 0.5}\left(\frac{0.0845}{4}\right)^2 = 1.68\times10^{-7}$$

For estimated life at higher propellant utilization efficiency, let $\eta_{u,\,chamber} = 89$ percent

$$J_0 = \frac{0.072}{0.89} = 81 \text{ MA}$$

$$n_0 = \frac{J_0 - J_B}{A_0 ev}$$

$$= \frac{0.081 - 0.072}{26.6\times 1.6\times10^{-19}\times 2\times10^4}$$

$$= \frac{9\times10^{-3}}{2.66\times 10\times 1.6\times10^{-19}\times 2\times10^4}$$

$$n_0 = 1.05\times10^{11}\ \frac{1}{cm^3}$$

$$I_{C.E.} = I_B \sigma n_0 l$$

$$= 6.05\times10^{-5}\times 6\times10^{-15}\times 1.05\times10^{11}\times 1.04$$

$$= 3.8\times10^{-8} \text{ A}$$

For a comparable degree of erosion,

$$M_{S.E.} = 4.56\times10^{-3} = Y_S \times \frac{I_{C.E.}}{e}\times w \times T$$

The expected lifetime is,

$$T = \frac{4.56\times10^{-3}\times 1.6\times10^{-19}}{0.5\times 3.8\times10^{-8}\times 16.1\times10^{-23}} \text{ sec}$$

$$= 23.8\times10^7 \text{ sec}$$

$$= 6.6\times10^4 \text{ hours}$$

Appendix B - Baffle Erosion Calculation

The mass of sputtered material per unit area, m_s, is given by

$$m_s = \rho \times t = \left(Y_s^+ \times n^+ \times v^+ + Y_s^{++} \times n^{++} \times v^{++}\right)\times w \times T$$

where

m_s = mass of sputtered material per unit area, g/cm^2

ρ = density of sputtered material, g/cm^3

t = thickness or depth of erosion, cm

Y_s^+ and Y_s^{++} = sputter yield for singly and doubly charged ion, respectively, atom/Hg ion

n^+ and n^{++} = number density of singly and doubly charged ions, respectively, ions/cm^3

v^+ and v^{++} = velocity of singly and doubly charged ions, respectively, cm/sec

w = mass per sputtered atom, g/atom

T = time, 5×10^7 sec

The electron number density at the discharge centerline is generally known to be about 1.6×10^{11} $1/cm^3$ of which 1×10^{11} $1/cm^3$ is at a Maxwellian temperature ranging from 3 to 10 eV and 0.6×10^{11} $1/cm^3$ are primaries at 40 eV (ref. 16).

The ratio of doubly to singly charged ions in the beam is generally 0.1 or less. The ratio of doubly to singly charged ions in the ion chamber can be related to the ratio in the beam by

$$\frac{n^{++}}{n^+} = \frac{I^{++}/I^+}{2\sqrt{2}} \quad \text{(ref. 16)}$$

where

$\frac{n^{++}}{n^+}$ = ratio of double to single ions in ion chamber

$\frac{I^{++}}{I^+}$ = ratio of double to single ions in the beam

Assuming that in a neutral plasma,

$$n_e = n^+ + 2n^{++}$$

$$n^{++} = \left(\frac{n^{++}}{n^+}\right)\left[\frac{n_e}{1 + 2\left(\frac{n^{++}}{n^+}\right)}\right]$$

where

n_e = electron number density, $1/cm^3$

For

$$\frac{n^{++}}{n^+} = \frac{0.1}{2\sqrt{2}} = 0.035$$

$$n^{++} = 5.24\times10^9 \text{ ion}/cm^3$$

and,

$$n^+ = n_e - 2n^{++}$$

$$= 1.5\times10^{11} \text{ ion}/cm^3$$

The Bohm velocity for ions at Maxwellian temperatures of 3 to 10 eV is,

$$v = 100\sqrt{\frac{T_{mx}q}{m_i}\left(1 + \frac{n_{pr}}{n_{mx}}\right)} \text{ cm/sec}$$

where

T_{mx} = Maxwellian temperature, eV

q = charge on ion, 1.6×10^{-19} coulomb per charge

m_i = mass of ion, 3.33×10^{-25} kg/atom

$\frac{n_{pr}}{n_{mx}}$ = ratio of primary to Maxwellian electron number density, 0.6

Then, for doubly charged ions,

$$v^{++} = 2.14\times10^5 \text{ to } 3.92\times10^5 \text{ cm/sec}$$

and for singly charged ions,

$$v^+ = 1.51\times10^5 \text{ to } 2.77\times10^5 \text{ cm/sec}$$

Using the following assumed values for graphite (refs. 12 and 13)

$$Y_s^+ = 1\times10^{-3} \text{ atom/ion}$$

$$Y_s^{++} = 1.5\times10^{-2} \text{ atom/ion}$$

$$w = 2\times10^{-23} \text{ g/atom}$$

$$\rho = 2.25 \text{ g/cm}^3$$

The mass of sputtered material per unit area of graphite is,

$$m_s = 3.95\times10^{-2} \text{ to } 7.24\times10^{-2} \text{ g/cm}^2$$

and the depth of erosion for graphite is

$$t = 1.75\times10^{-2} \text{ to } 3.22\times10^{-2} \text{ cm}$$

Using the following assumed values for tantalum (refs. 12 and 13)

$$Y_s^+ = 7\times10^{-4} \text{ atom/ion}$$

$$Y_s^{++} = 2\times10^{-2} \text{ atom/ion}$$

$$w = 30\times10^{-23} \text{ g/atom}$$

$$\rho = 16.6 \text{ g/cm}^3$$

The sputtered mass per unit area of tantalum is,

$$m_s = 0.574 \text{ to } 1.052 \text{ g/cm}^2$$

and the depth of erosion for tantalum is,

$$t = 3.46\times10^{-2} \text{ to } 6.34\times10^{-2} \text{ cm}$$

The above analysis indicates that approximately 43 percent of the graphite sputter erosion and 59 percent of the tantalum sputter erosion is due to double ions, with the remainder of each due to single ion sputtering.

References

1. Nakanishi, S. and Finke, R. C., "A 9700-Hour Durability Test of a Five-Centimeter Diameter Ion Thruster," AIAA Paper No. 73-1111, Lake Tahoe, Nev., Oct.-Nov. 1973.

2. Collett, C., "Thruster Endurance Test," Hughes Research Labs., Malibu, Ca., May 1976; Available as CR-135011, NASA.

3. Wintucky, E., "Cycle Life Testing of 8-cm Mercury Ion Thruster Cathodes," AIAA Paper No. 76-986 (to be presented at this conference), Nov. 1976.

4. Mantenieks, M., "Status of 30 cm Mercury Ion Thruster Isolators," AIAA Paper No. 76-1027 (to be presented at this conference), Nov. 1976.

5. Kerslake, W. R., "Status of SERT-II Ion Thruster and Spacecraft - 1976," AIAA Paper No. 76-1061 (to be presented at this conference), Nov. 1976.

6. "8-Centimeter Mercury Ion Thruster Systems Technology," AIAA Paper No. 74-1116, Oct. 1974.

7. Nakanishi, S. and Finke, R. C., "A 2000-Hour Durability Test of a 5-Centimeter-Diameter Mercury Bombardment Ion Thruster," TM X-68155, 1972, NASA.

8. Hyman, J., Jr., et al., "One-Millipound Mercury Ion Thruster," AIAA Paper No. 75-386, Mar. 1975.

9. Aston, G., "The Ion-Optics of a Two-Grid Electron Bombardment Thruster," Colorado State Univ., Fort Collins, Col., May 1976; Available as CR-135034, NASA.

10. Ward, J. W. and King, H. J., "Life Limitations of Ion Extraction Systems," AIAA Paper No. 72-477, Apr. 1972.

11. Power, J. L. and Rotnem, J. O., "Operation of a Small Mercury Ion Thruster System in a Simulated Stationkeeping Mode Using a Microprocessor," AIAA Paper No. 76-995 (to be presented at this conference), 1976.

12. Wehner, G. K., "Sputtering Yields for Normally Incident Hg^+ Ion Bombardment at Low Energy," Physical Review, Vol. 108, Oct. 1957, pp. 35-45.

13. Askerov, Sh.G. and Sena, L. A , "Cathode Sputtering of Metals by Slow Mercury Ions," Soviet Physics - Solid State, Vol. 11, Dec. 1969, pp. 1288-1293.

14. Mantenieks, M. and Rawlin, V. K., "Sputtering Phenomena of Discharge Chamber Components in a 30-Centimeter Mercury Ion Thruster," AIAA Paper No. 76-988 (to be presented at this conference), Nov. 1976.

15. Weigand, A. J., "Operating Characteristics of a Hollow-Cathode Neutralizer for 5- and 8-Centimeter-Diameter Electron-Bombardment Mercury Ion Thruster," TM X-3209, 1975, NASA.

16. Peters, R. R., "Double Ion Production in Mercury Ion Thrusters," Colorado State Univ., Fort Collins, Col., Apr. 1976; Available as CR-135019, NASA.

TABLE I. - PERFORMANCE PROFILE

Test hours	5500	10,000	15,000
Anode voltage, V	1240	1250	1247
Accelerator potential, V	-500	-500	-530
Neutralizer floating potential, V	-32.6	-26.4	-20.8
Beam power, W	86.5	88.1	88.4
Discharge power, W	28.0	29.3	28.1
Component power:			
Accelerator drain, W	0.33	0.35	0.37
Cathode:			
Heater, W	0	0	0
Keeper, W	3.52	3.03	2.97
Vaporizer, W	5.39	6.66	6.19
Neutralizer:			
Heater, W	7.2	7.2	7.2
Keeper, W	9.35	9.24	8.8
Vaporizer, W	0.72	0.73	0.89
Total input power, W	141.0	144.6	142.9
Power efficiency, percent	61.3	60.9	61.9
Utilization efficiency, percent	59.3	61.3	64.0
Overall efficiency, percent	36.4	37.3	39.6
Thrust, mN	5.08	5.12	5.11
Specific impulse, sec	2056	2144	2240
P/T ratio, W/mN	27.8	28.2	28.0

E-8866

TABLE II. - THRUSTER COMPONENT WEIGHT ANALYSIS

Component	Test hours		Change, gm
	1156	15,040	
	Weights, gm		
Accelerator grid and mount ring	131.5766	127.7722	-3.8044
Screen grid and mount ring	154.8165	155.5783	+0.7618
Screen pole piece	49.0751	48.8215	-0.2536
Grid assembly (all parts)	465.7450	462.4460	-3.0290
Thruster body	23.6759	23.8206	+0.1147
Anode	22.5854	23.5140	+0.9286
Graphite baffle assembly	0.45217	0.4071	-0.04507
Graphite back plate	9.47752	8.8937	-0.5838
Cathode pole piece	23.51614	23.3669	-0.1492
Cathode ignitor electrode	1.51850	1.4193	-0.0992
Cathode ignitor lock nut	0.81509	0.8043	-0.01079
Cathode ignitor shadow shield	1.80178	1.7369	-0.06488
Neutralizer ignitor	2.35598	2.3373	-0.01868

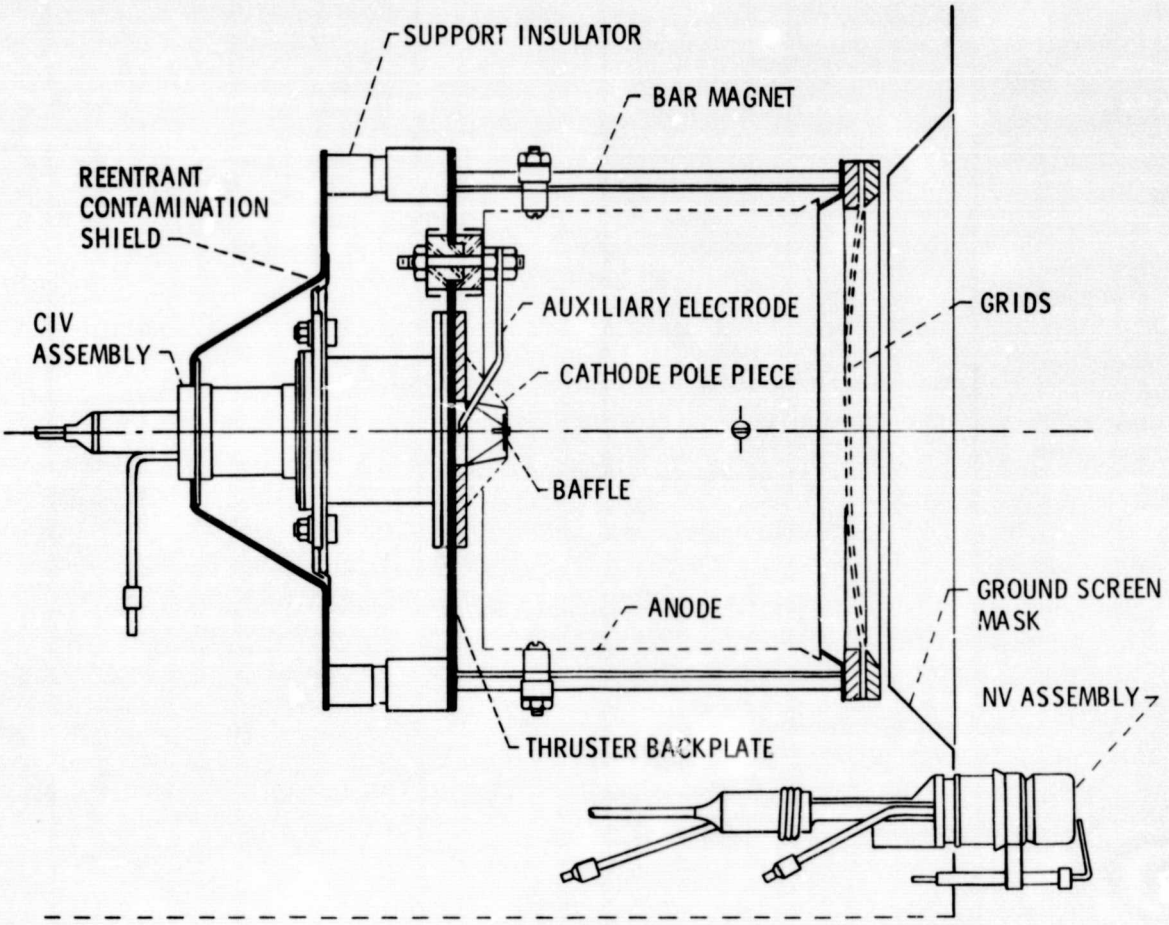

Figure 1. - Cross-section view of laboratory model 8 centimeter thruster.

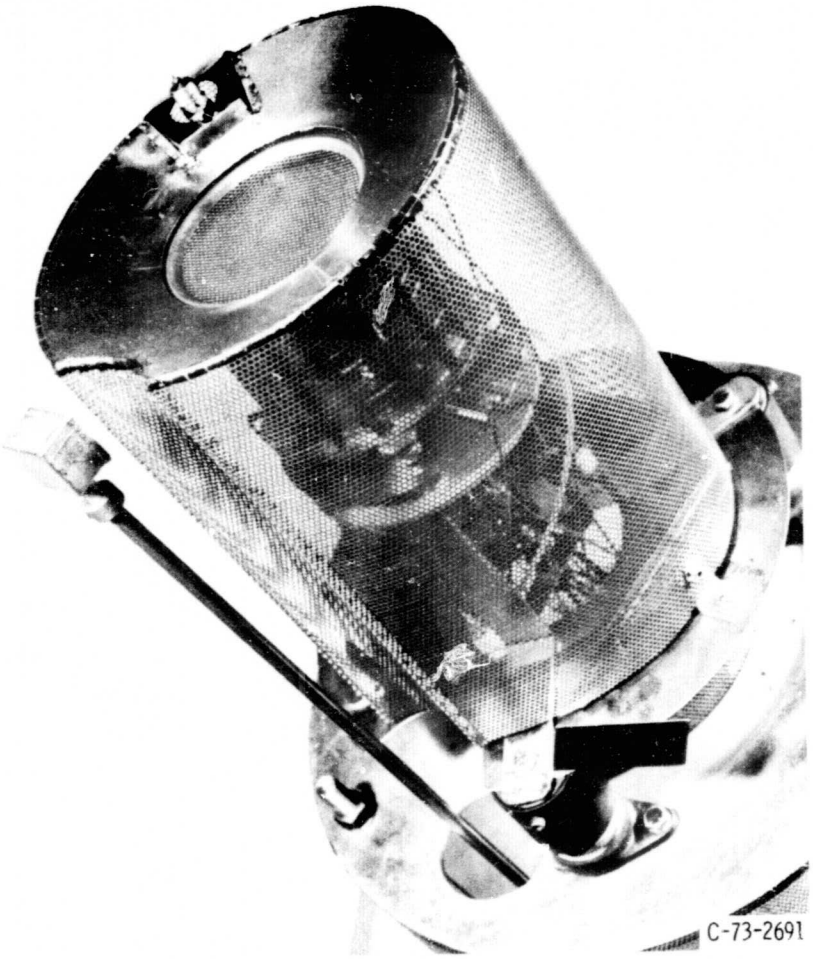

Figure 2. - 8 cm diameter ion thruster mounted for cyclic endurance testing.

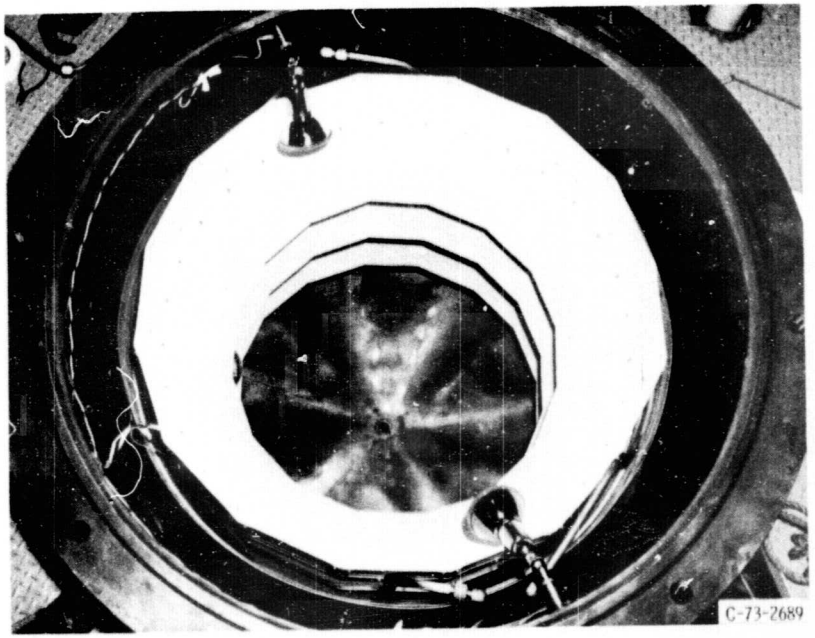

Figure 3. - Interior of vacuum test facility prior to test.

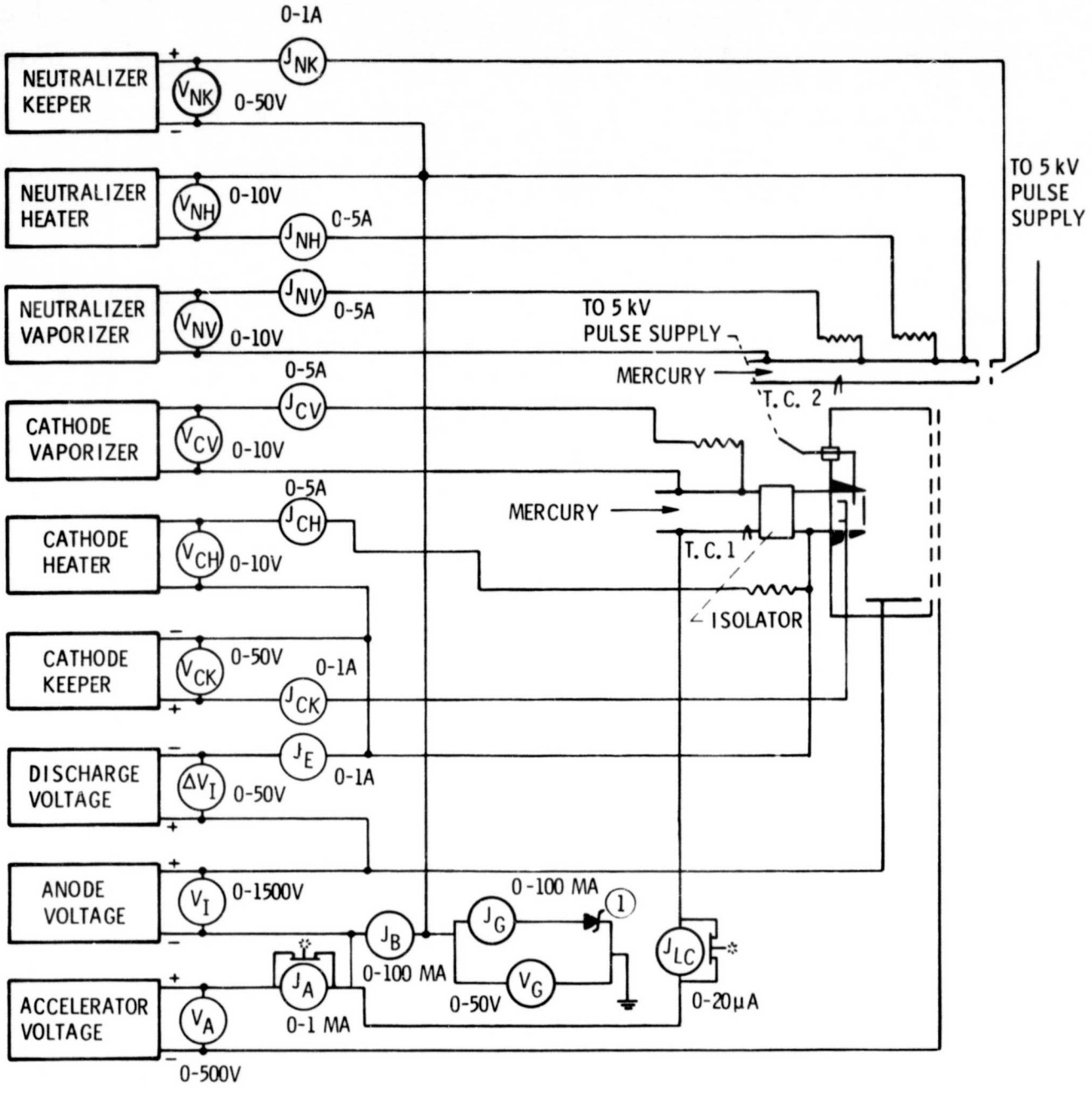

NOTES:

* METER NORMALLY SHUNTED WITH CLOSED SWITCH. PUSH TO READ.

T. C. IRON CONSTANTAN THERMOCOUPLE

(1) ZENER DIODE, 50 V, 20 W.

Figure 4. - Wiring schematic for 1 mlb ion thruster.

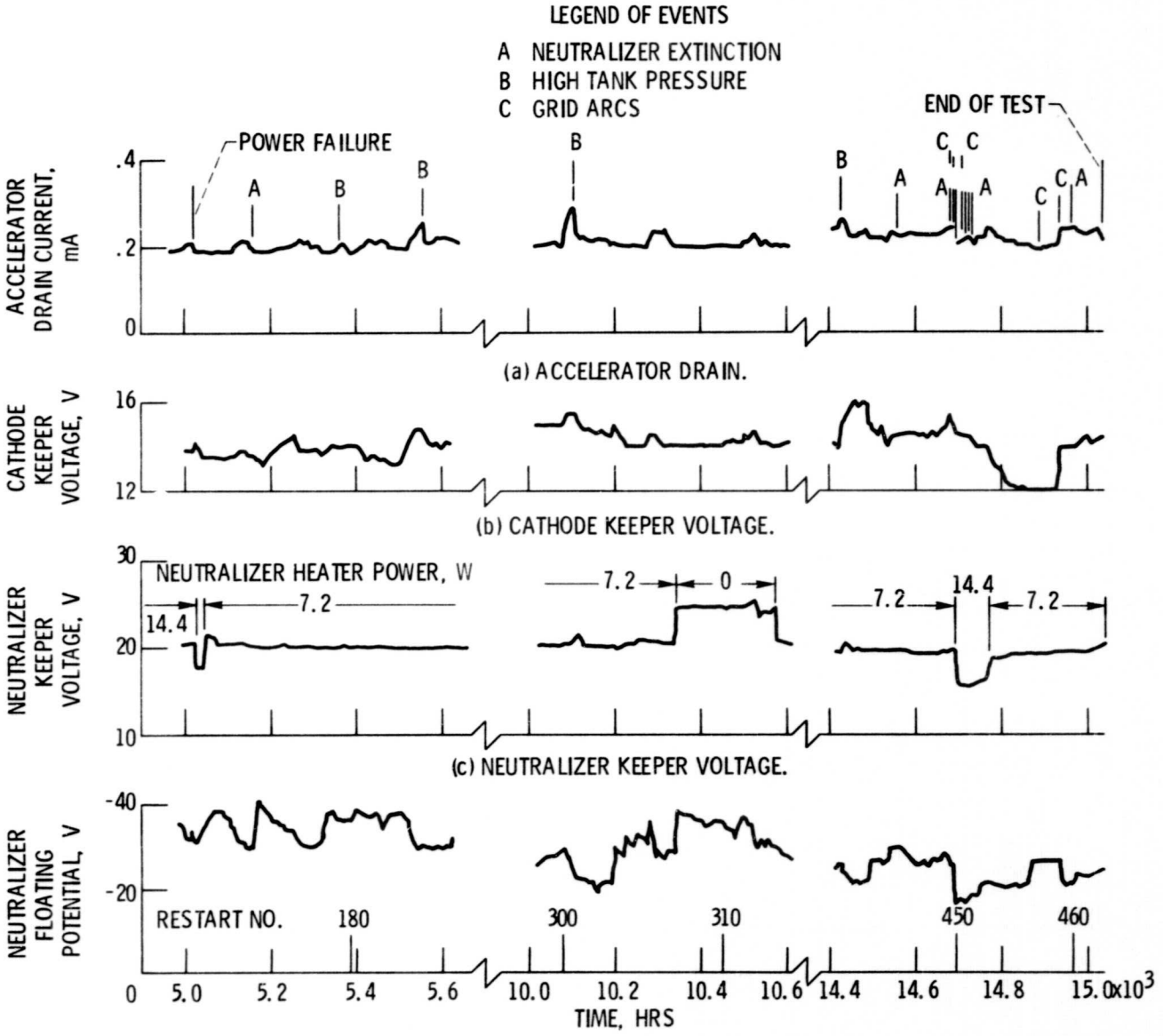

Figure 5. - Time history segments of cyclic endurance test.

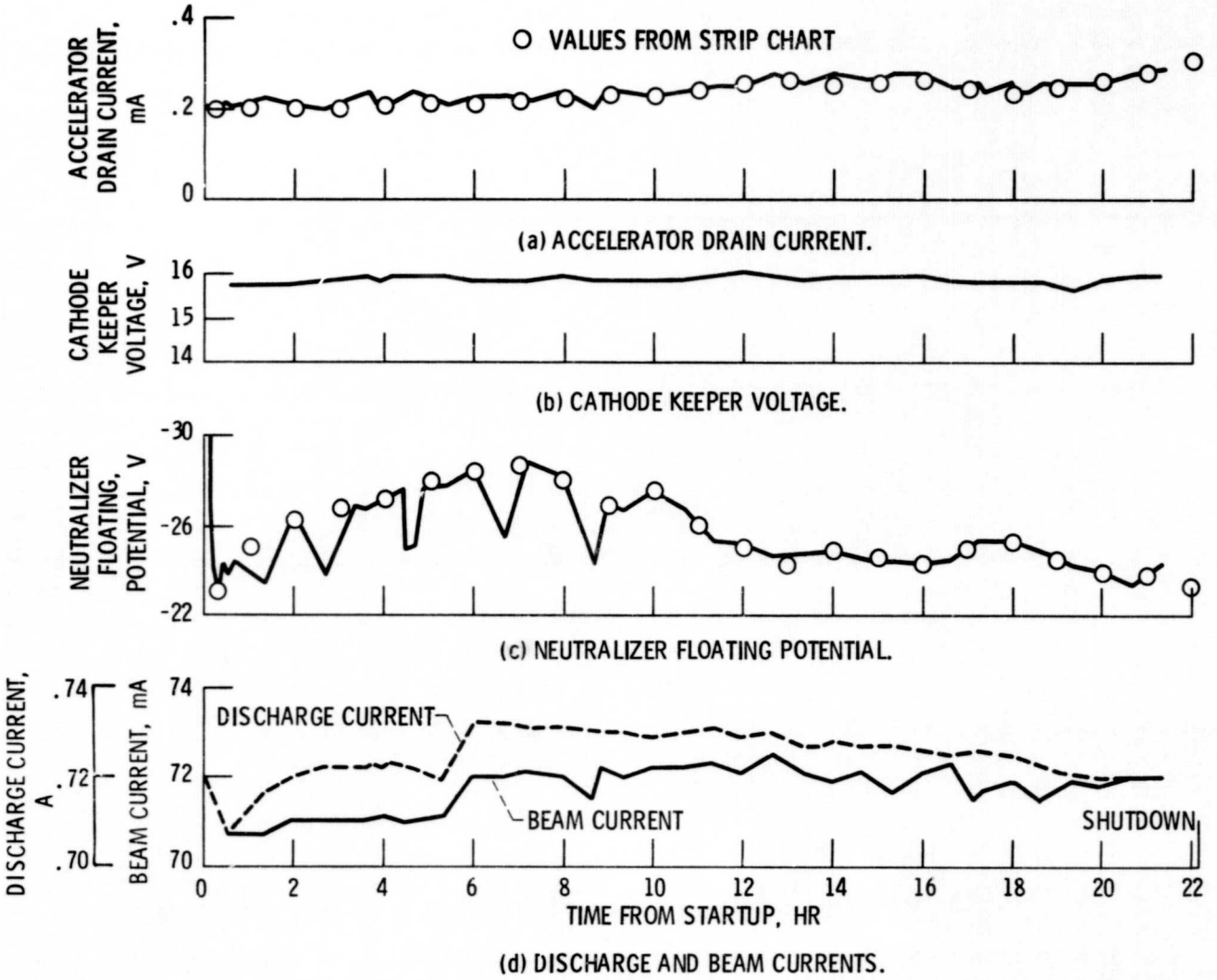

Figure 6. - Typical digitized record of transient from startup to shutdown of a cycle; thruster time, 10,081 hours.

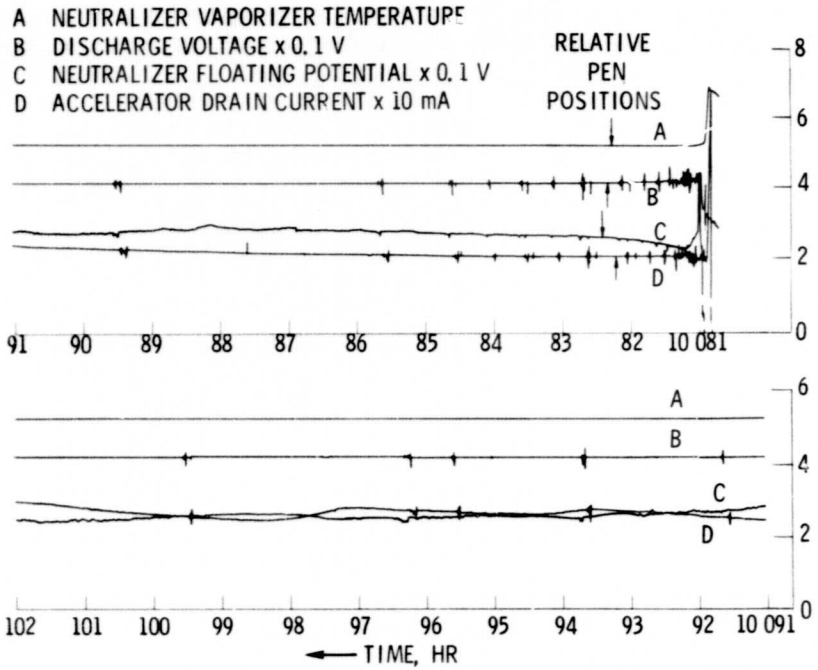

Figure 7. - Continuous strip chart record of a typical on-off cycle.

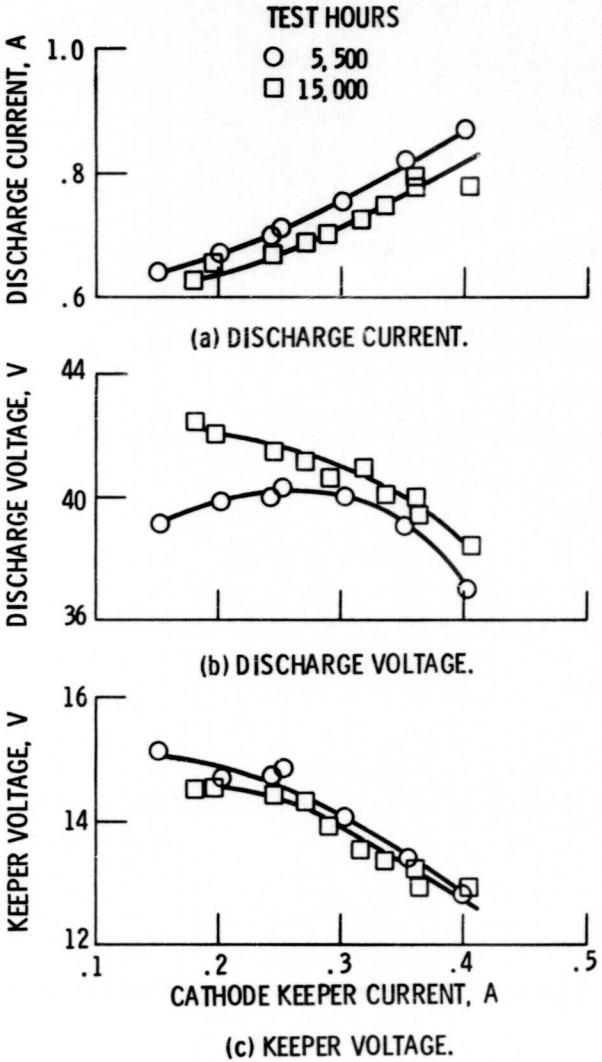

Figure 8. - Effects of varying cathode keeper current; beam current, 72 mA.

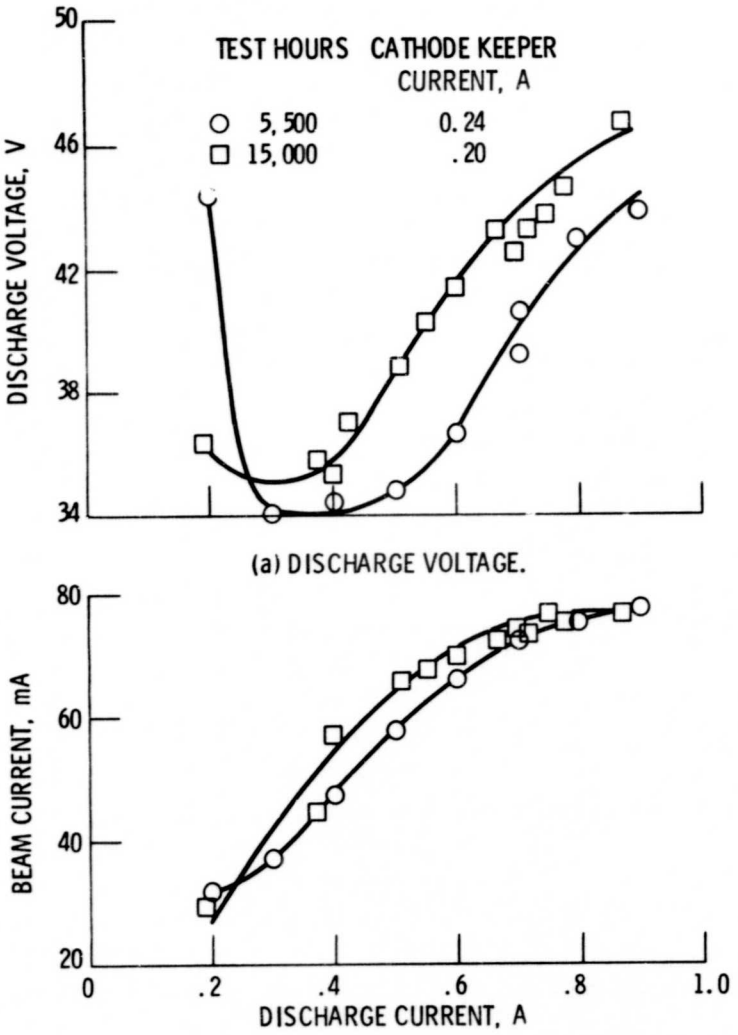

(a) DISCHARGE VOLTAGE.

(b) BEAM CURRENT.

Figure 9. Effects of varying discharge current.

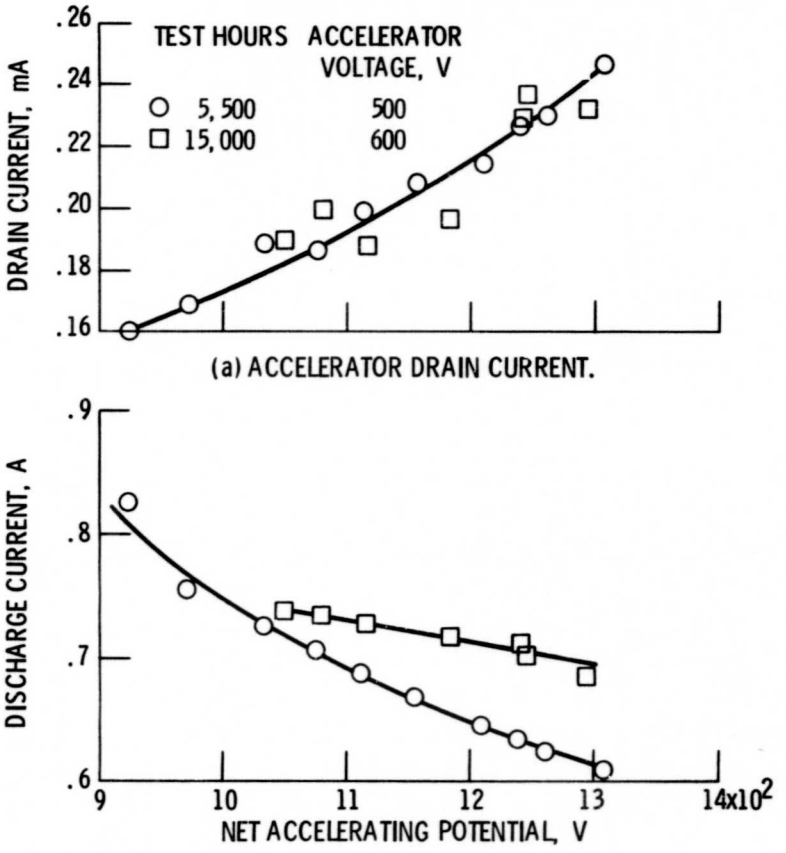

(a) ACCELERATOR DRAIN CURRENT.

(b) DISCHARGE CURRENT.

Figure 10. - Effects of varying net accelerating potential; beam current, 72 mA.

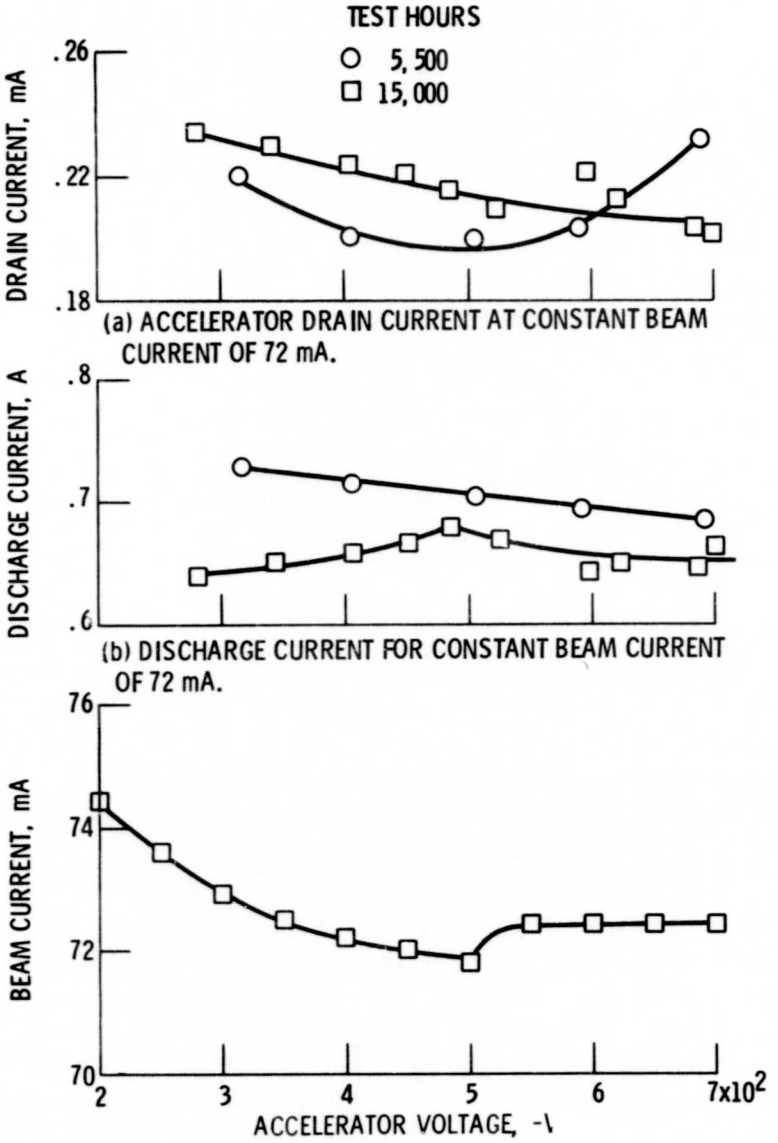

(a) ACCELERATOR DRAIN CURRENT AT CONSTANT BEAM CURRENT OF 72 mA.

(b) DISCHARGE CURRENT FOR CONSTANT BEAM CURRENT OF 72 mA.

(c) BEAM CURRENT AT CONSTANT DISCHARGE CURRENT OF 0.65 A.

Figure 11. - Effects of varying accelerator voltage; net accelerating potential, 1250 V.

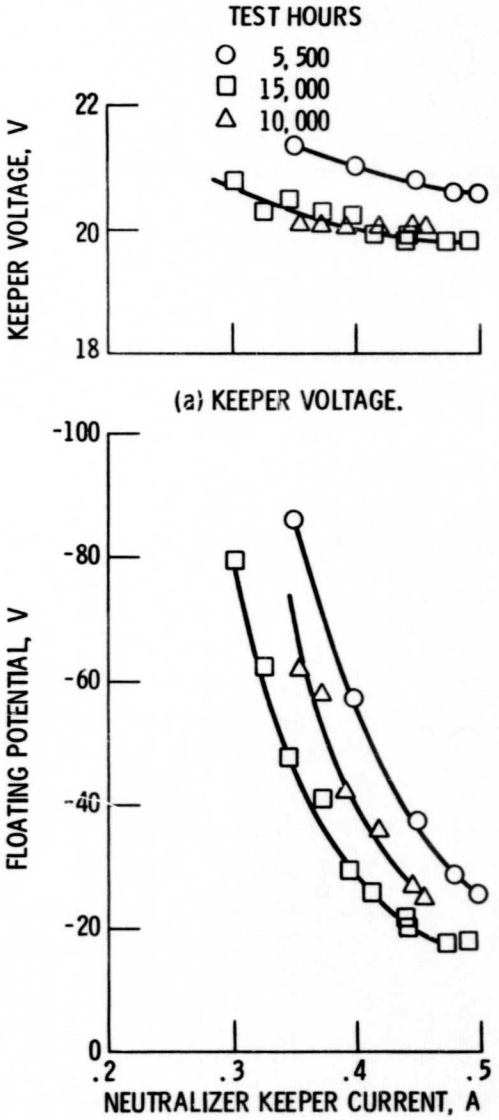

(a) KEEPER VOLTAGE.

(b) NEUTRALIZER FLOATING POTENTIAL.

Figure 12. - Effects of varying neutralizer keeper current; beam current, 72 mA; neutralizer heater power, 7.2 W.

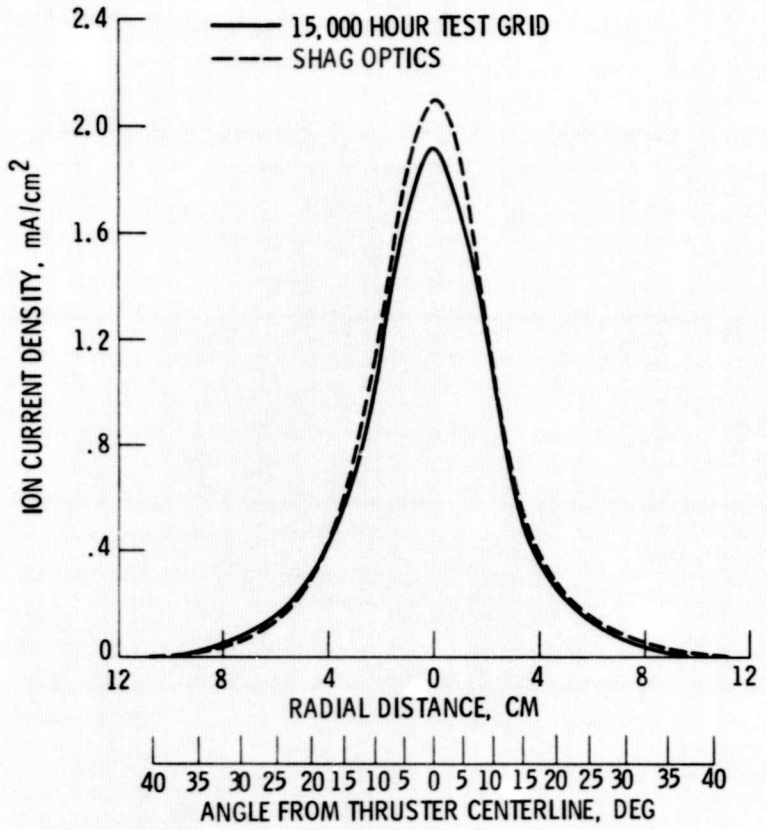

Figure 13. - Ion beam current density profile at axial distance of 12.7 cm; beam current, 72 mA; net accelerating potential, 1250 V; accelerator voltage, -500 V.

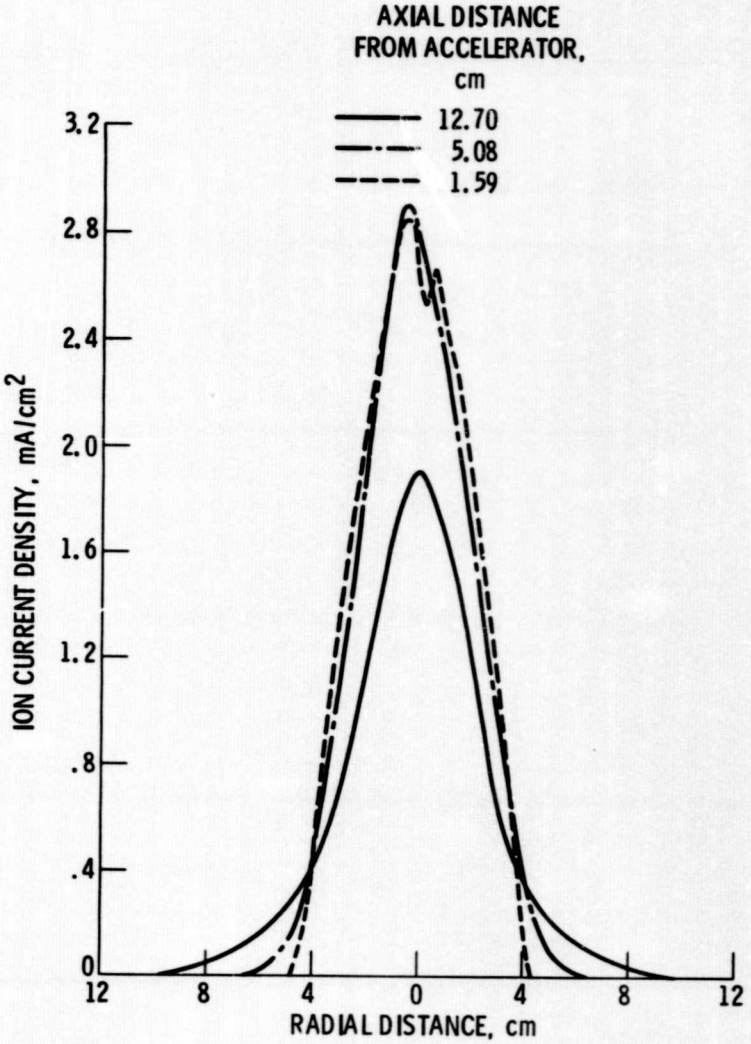

Figure 14. - Ion beam current density downstream of accelerator; beam current, 72 mA; net accelerating potential, 1250 V, accelerator voltage, -500 V.

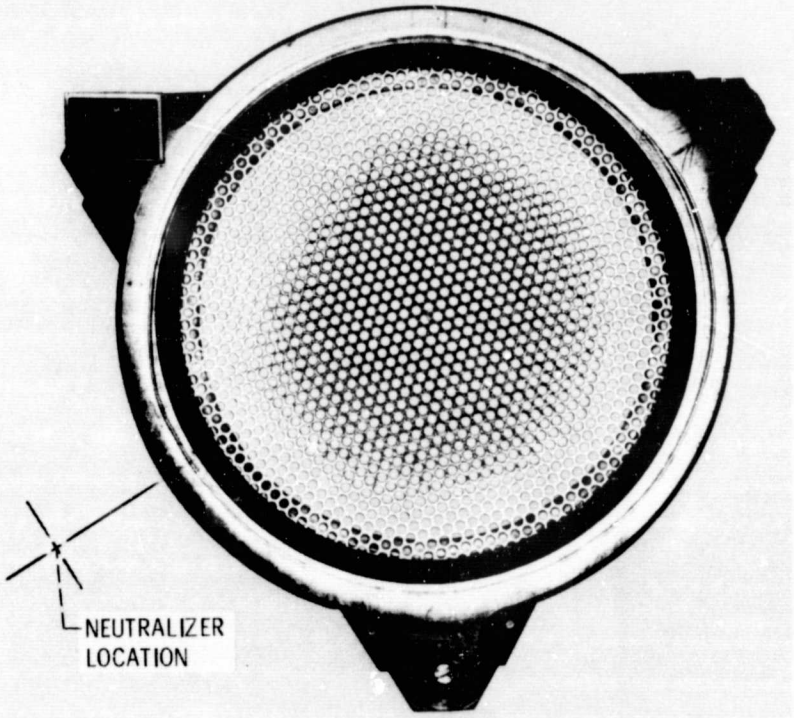

C-75-4162

Figure 15. - Downstream face of accelerator grid after 15 000 hour test.

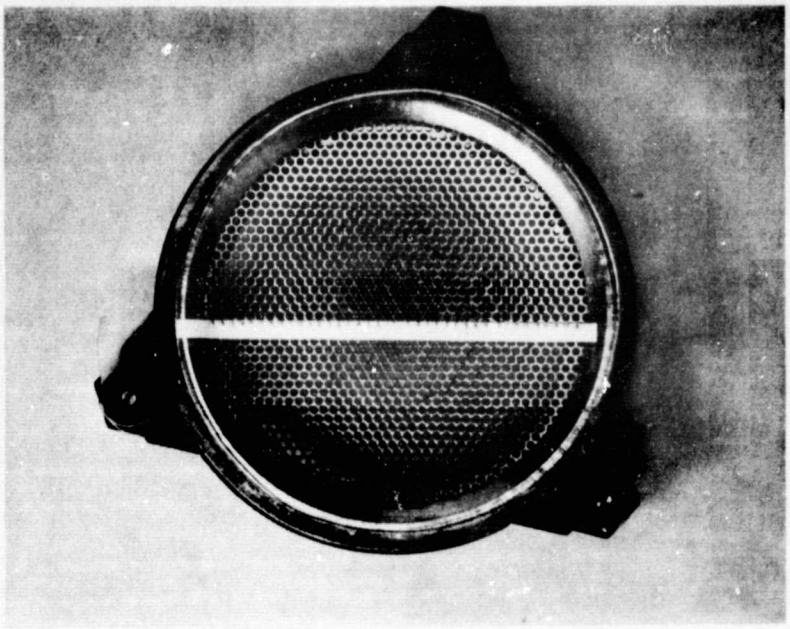

(a) ARRAY OF ACCELERATOR HOLES EXAMINED.

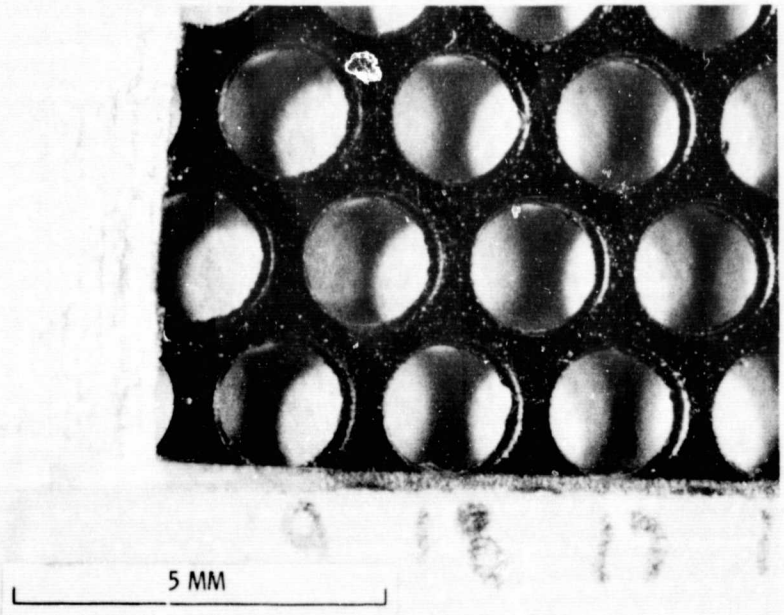

(b) HOLES 19 TO 17 AND MM SCALE.

Figure 16. - Close-up of accelerator.

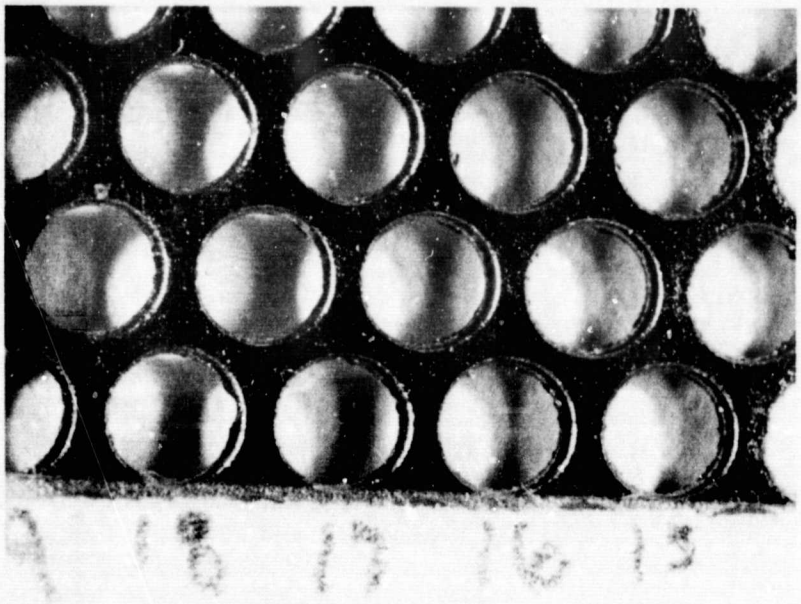

(c) HOLES 18 TO 15.

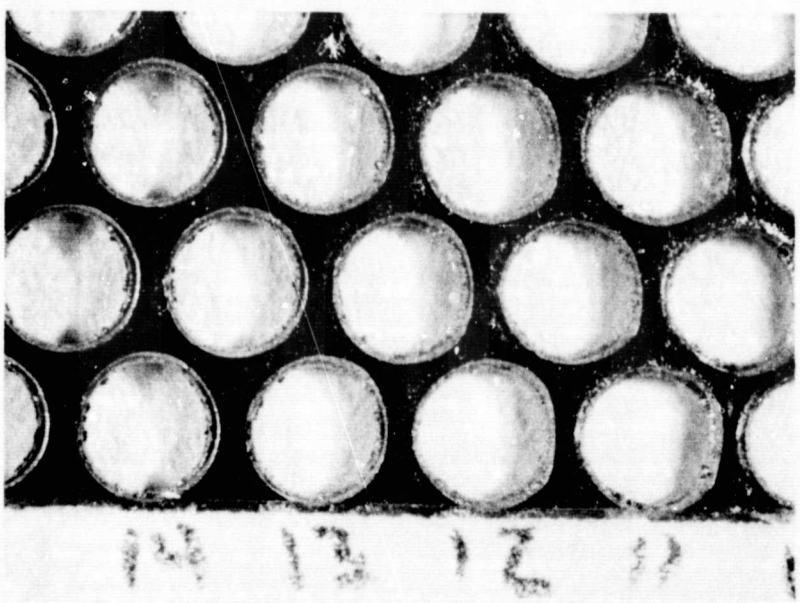

(d) HOLES 14 TO 11.

Figure 16. - Continued.

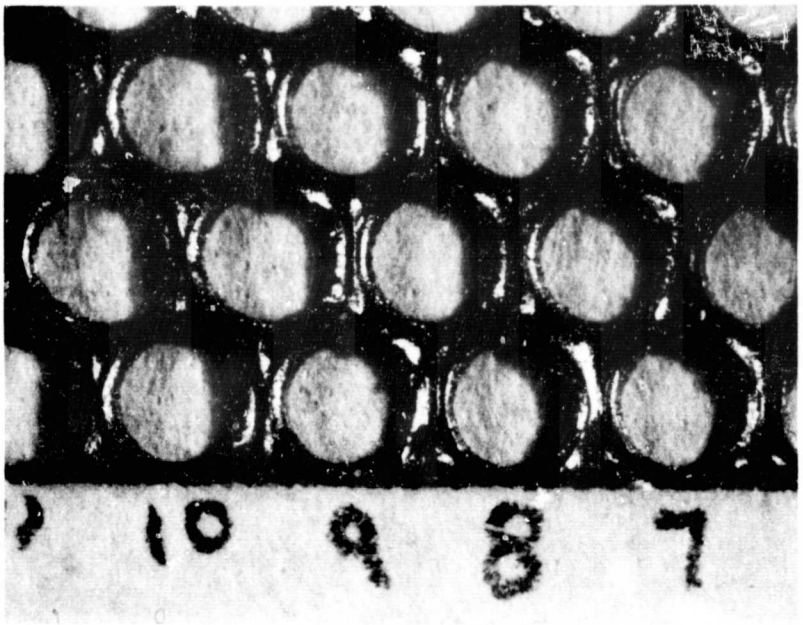

(e) HOLES 10 TO 7.

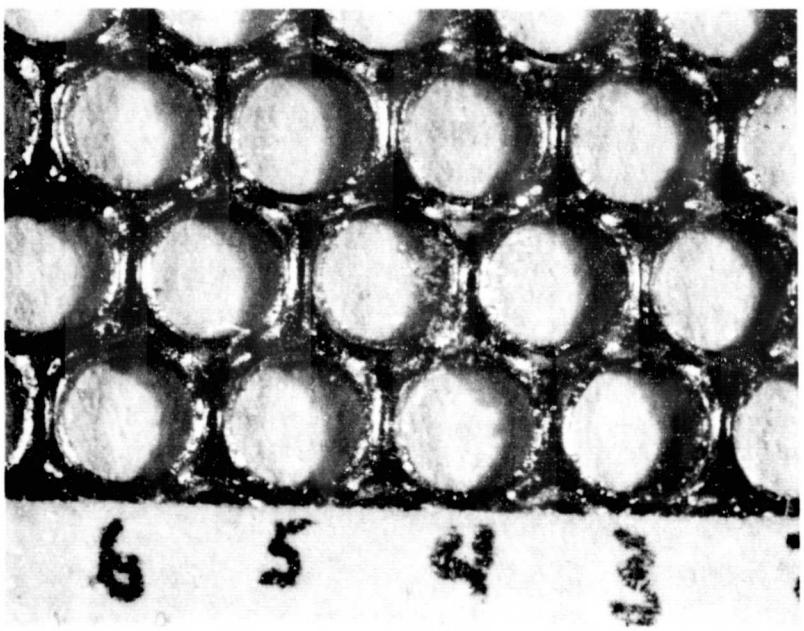

(f) HOLES 6 TO 3.

Figure 16. - Continued.

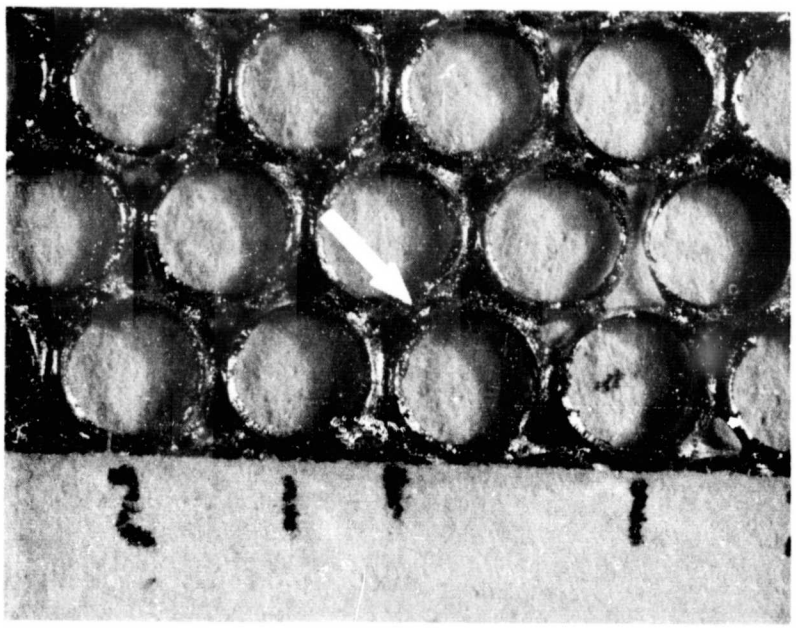

(g) HOLES 2, 0 AND 1.

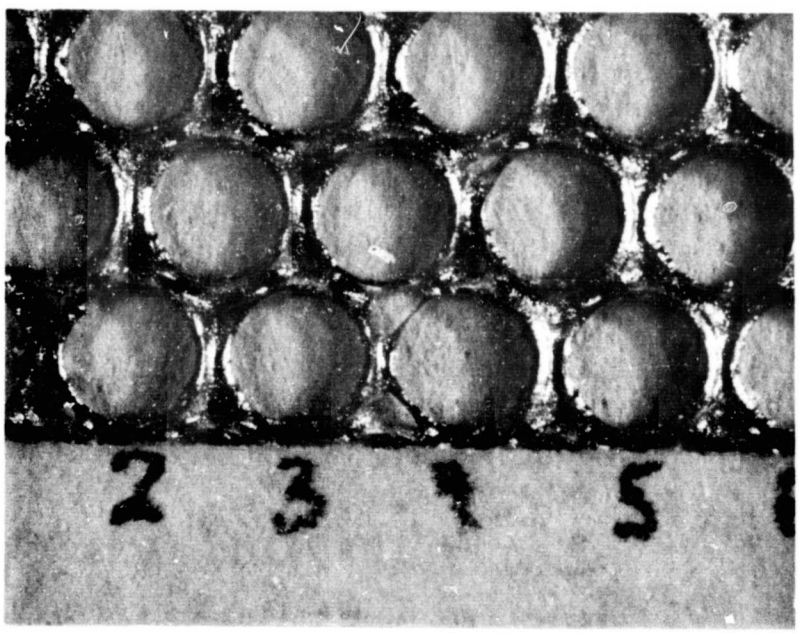

(h) HOLES 2 TO 5.

Figure 16. - Continued.

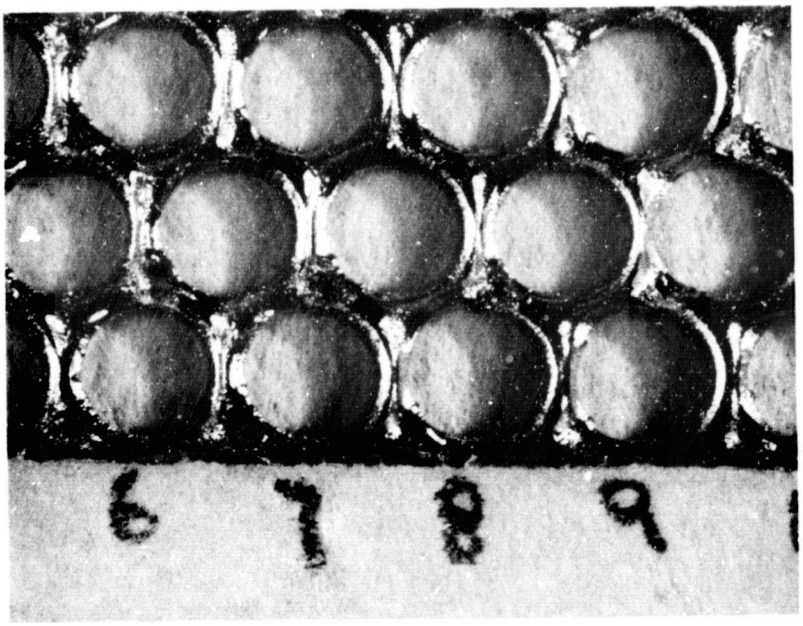

(i) HOLES 6 TO 9.

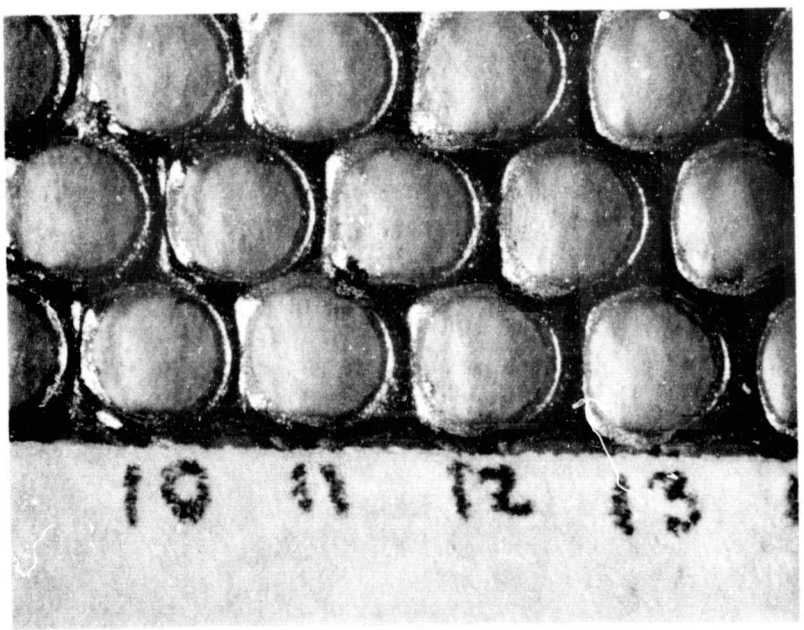

(j) HOLES 10 TO 13.

Figure 16. - Continued.

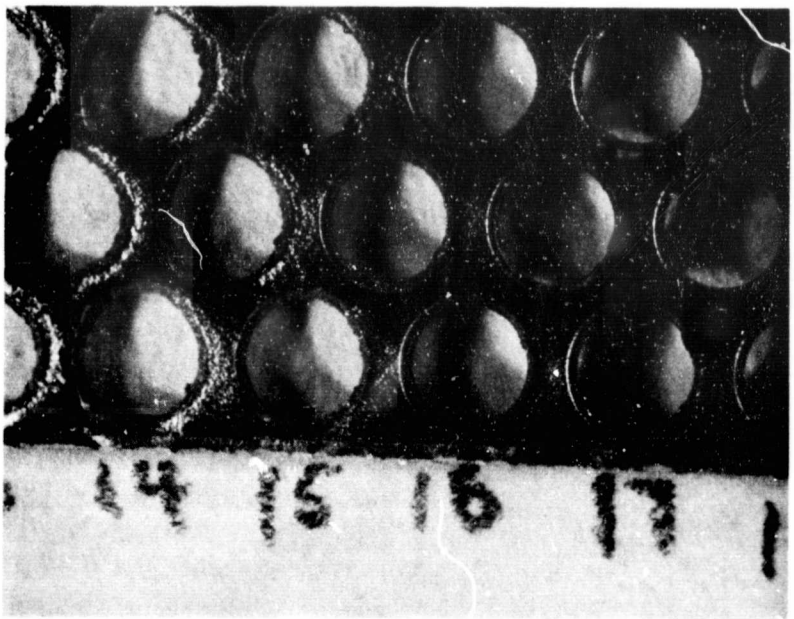

(k) HOLES 14 TO 17.

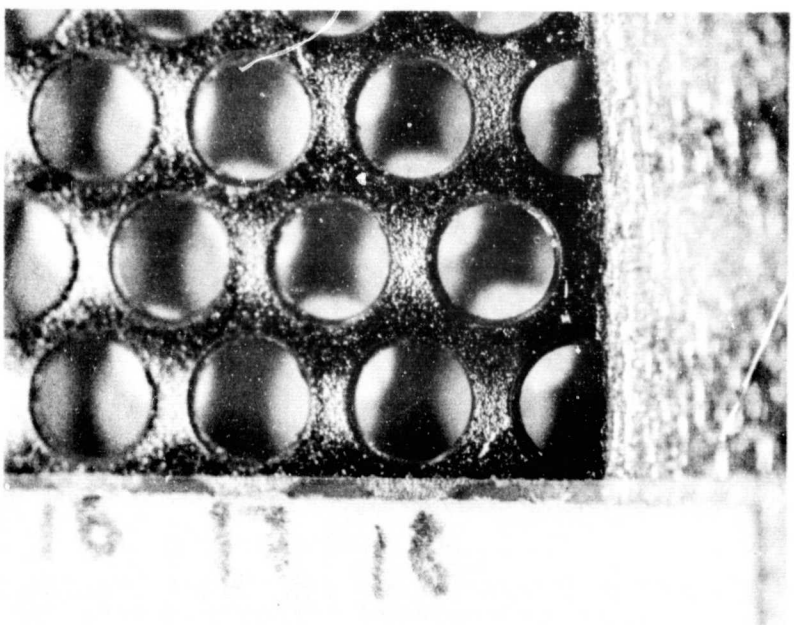

(l) HOLES 16 TO 18.

Figure 16. - Concluded.

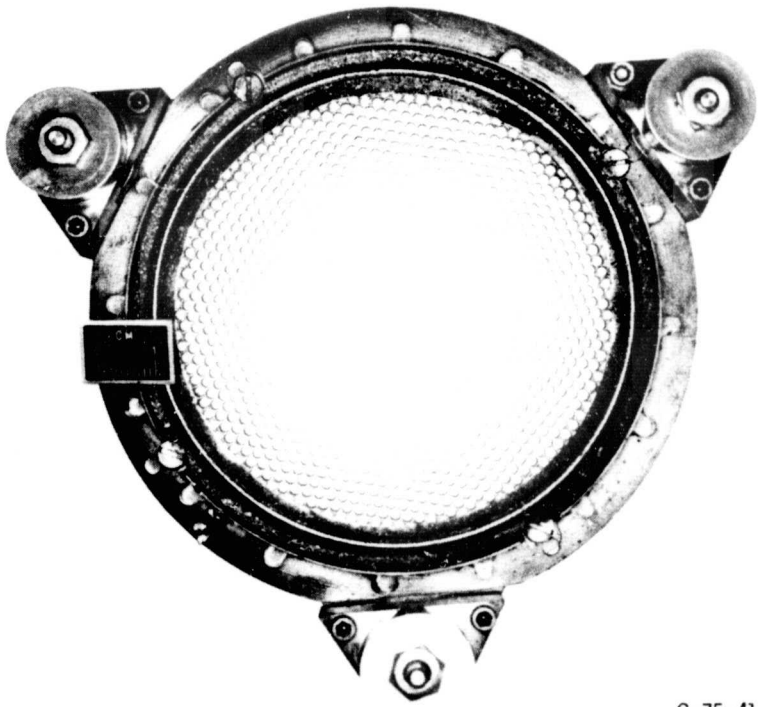

C-75-4161

Figure 17. - Upstream side of screen grid after 15 000 hour test.

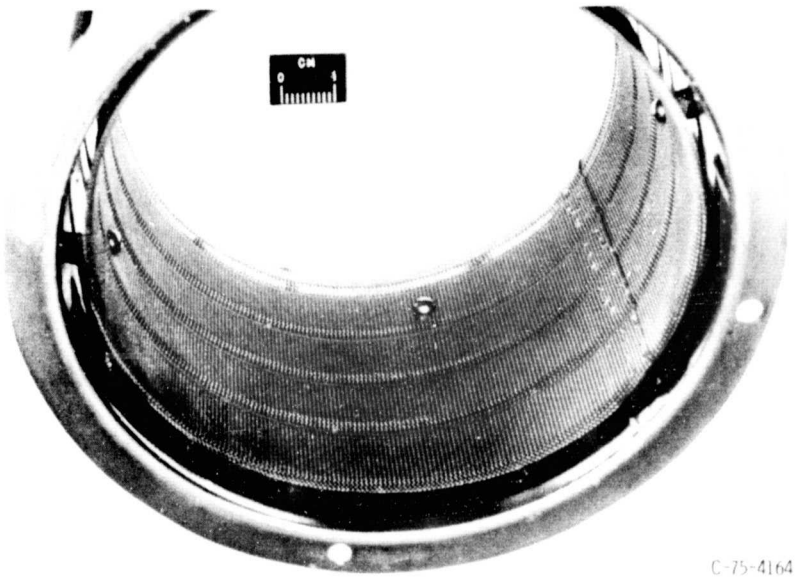

C-75-4164

Figure 18. - Screen anode after 15 000 hour test.

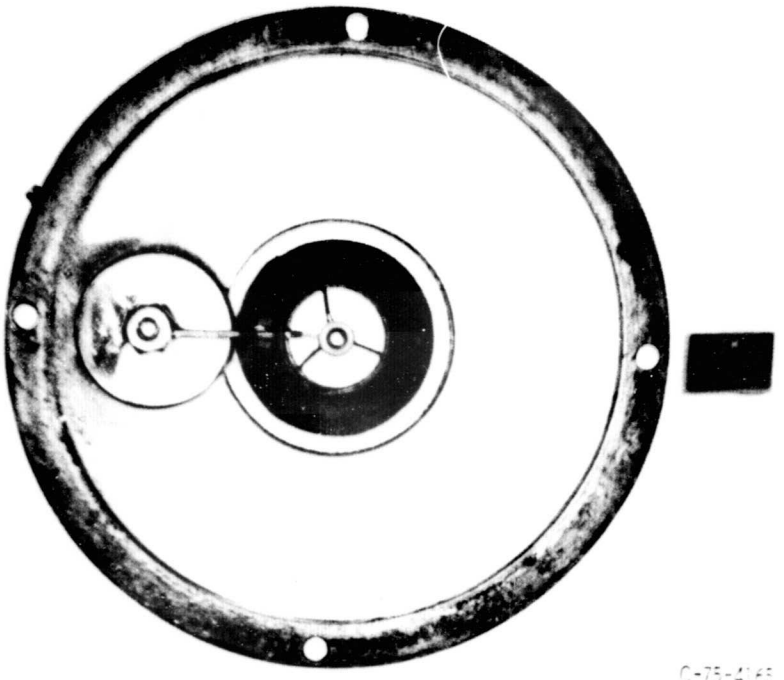

C-75-4165

Figure 19. - Thruster back plate and cathode pole - baffle assembly.

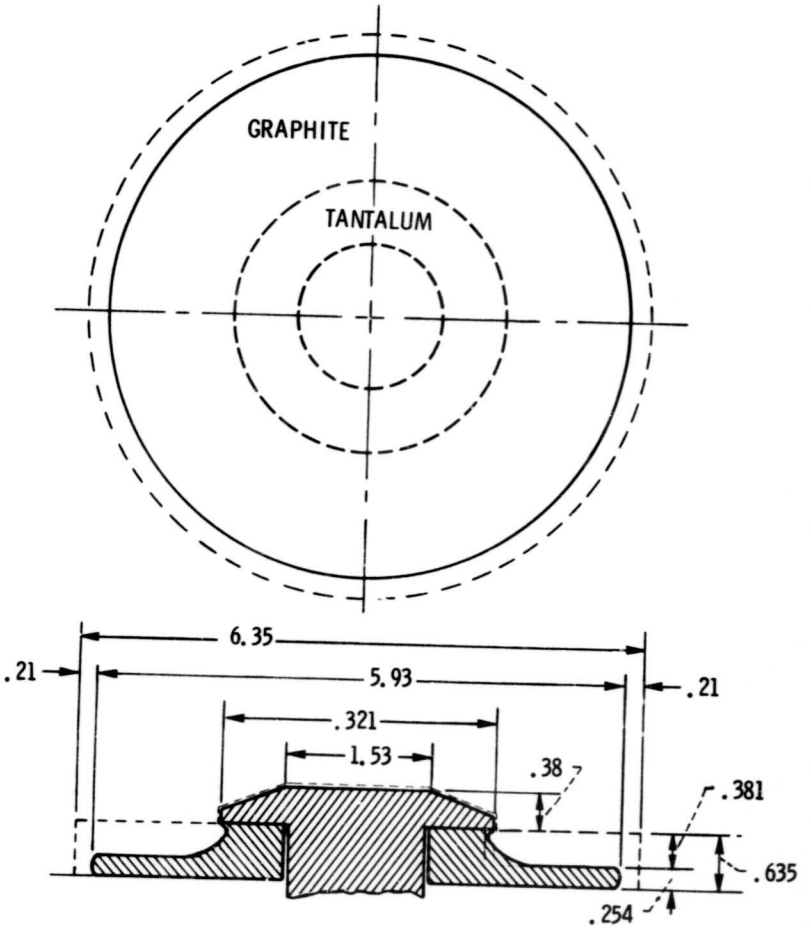

NOTE: ALL DIMENSIONS IN MILLIMETERS
DOTTED OUTLINE WHEN NEW

Figure 20. - Enlarged drawing of baffle assembly.

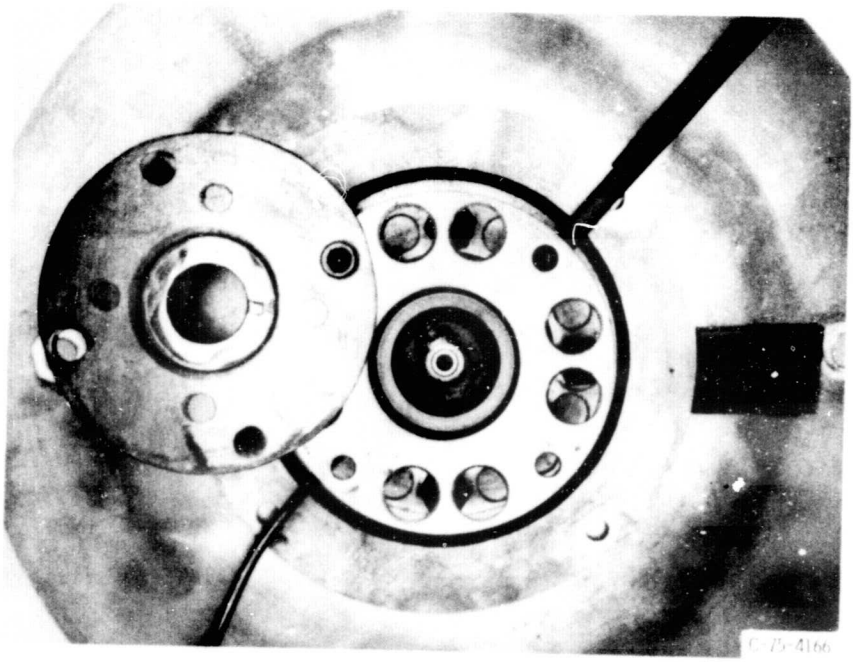

Figure 21. - Cathode assembly after 15 000 hour test.

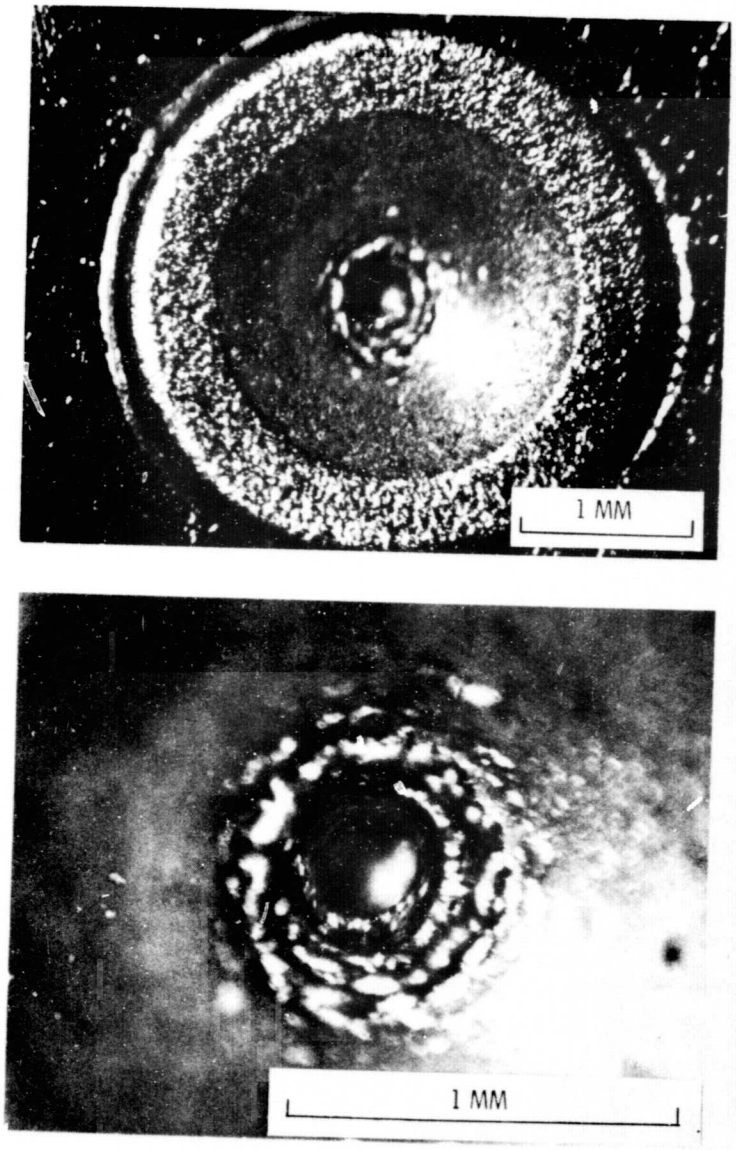

Figure 22. - Photomicrographs of cathode tip after 15 000 hours.

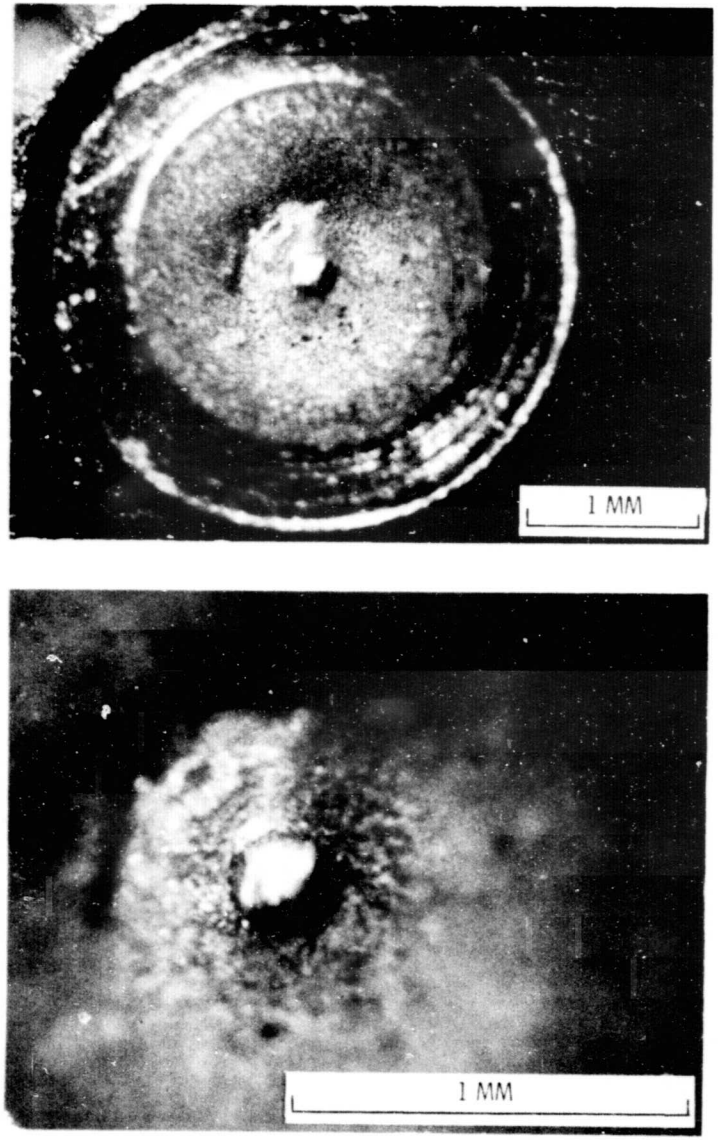

Figure 23. - Photomicrographs of cathode tip after 1156 hours.

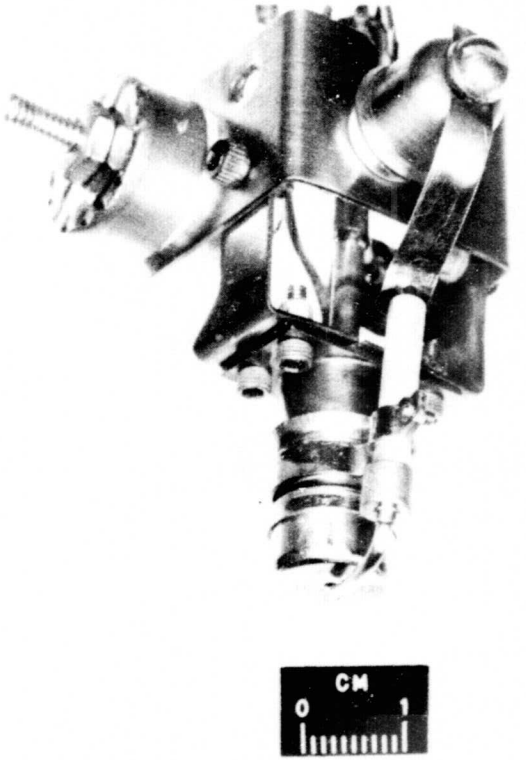

C-75-4163

Figure 24. - Neutralizer assembly after 15 000 hour test.

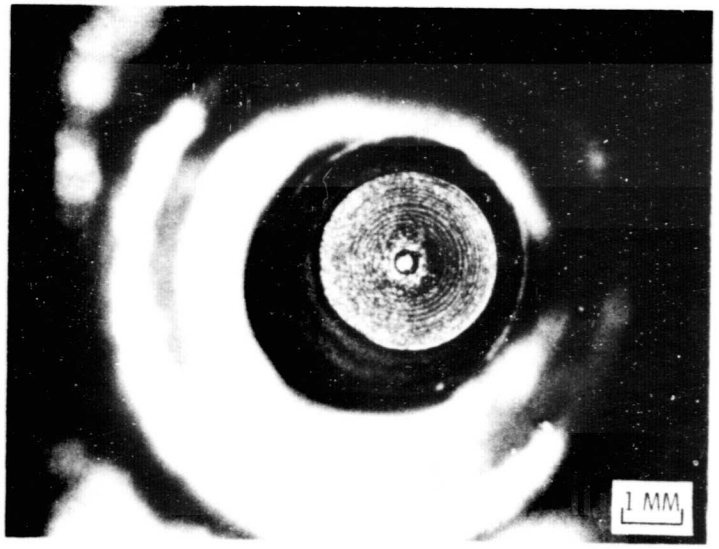

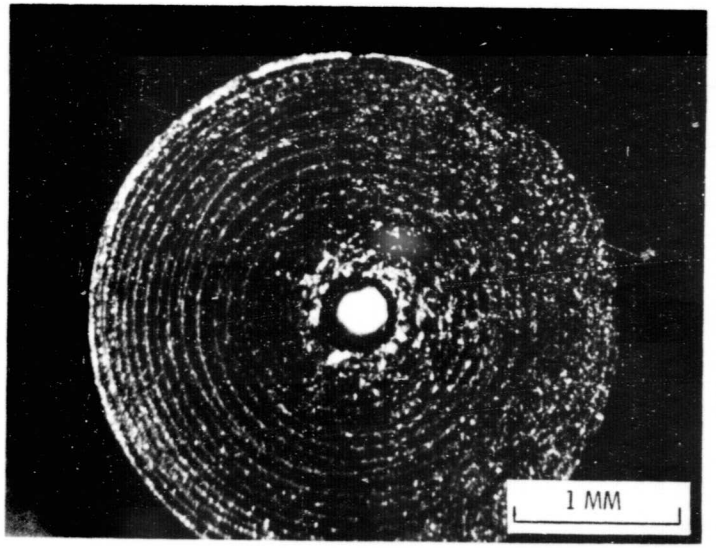

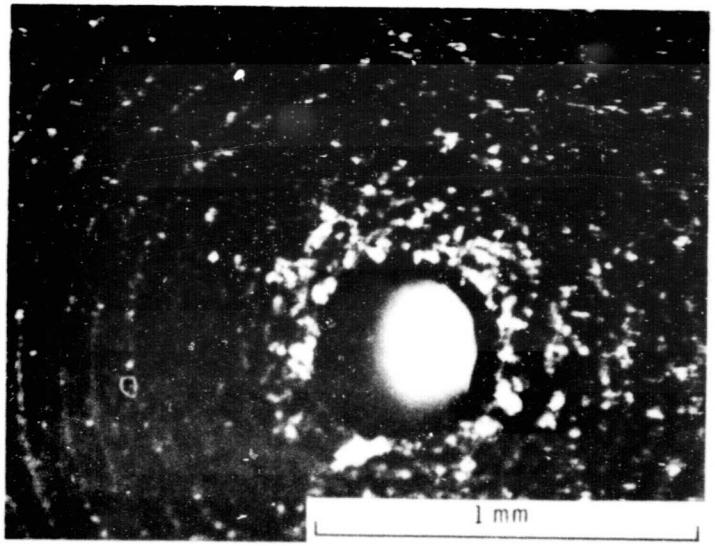

Figure 25. - Microphotographs of neutralizer tip after 15 000 hour test.

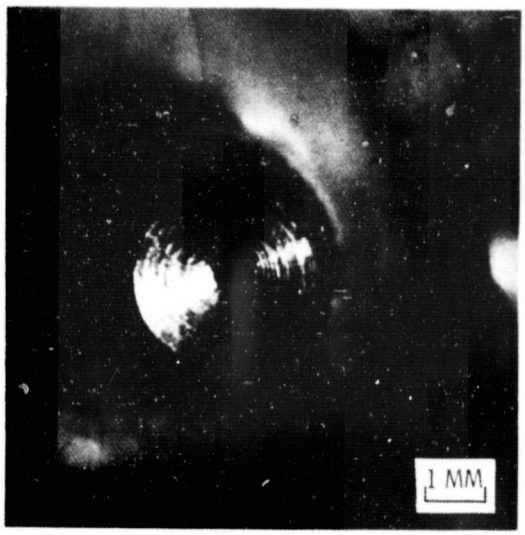

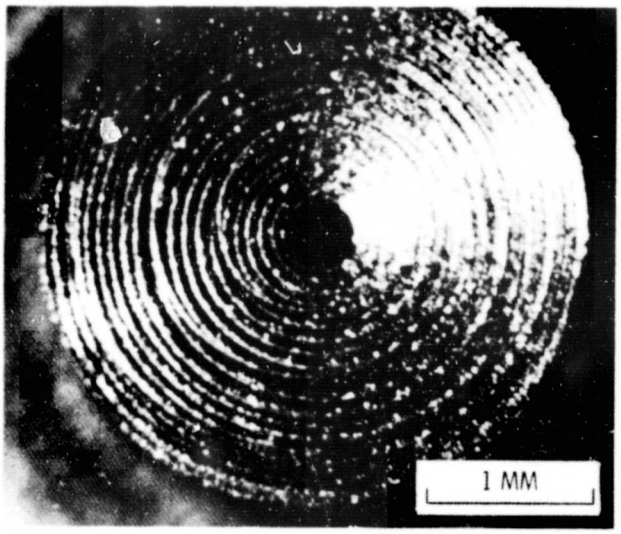

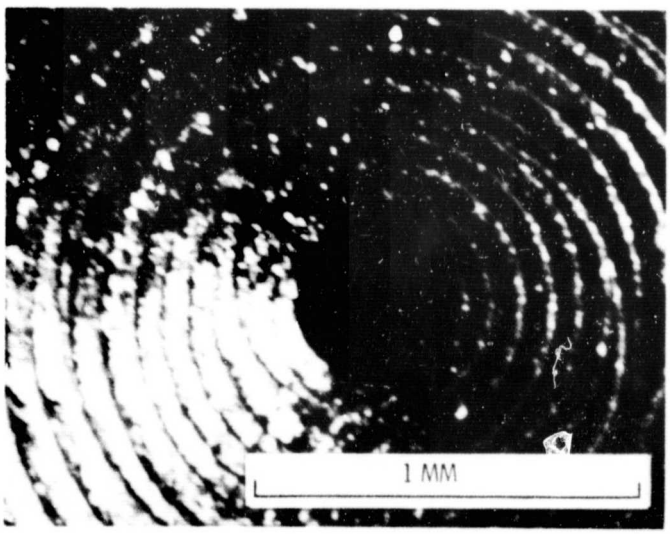

0.34 MM< ORIFICE DIAMETER <0.37 MM

Figure 26. - Microphotographs of neutralizer tip after 1156 hours of operation.

E-8866

NASA-Lewis